

Light nuclides produced in the proton-induced spallation of ^{238}U at 1 GeV

M. V. Ricciardi,¹ P. Armbruster,¹ J. Benlliure,² M. Bernas,³ A. Boudard,⁴ S. Czajkowski,⁵
T. Enqvist,¹ A. Kelić,¹ S. Leray,⁴ R. Legrain,⁴ B. Mustapha,³ J. Pereira,² F. Rejmund,¹ K.-H. Schmidt,¹
C. Stéphan,³ L. Tassan-Got,³ C. Volant,⁴ and O. Yordanov¹

¹*GSI, Planckstr. 1, D-64291 Darmstadt, Germany*

²*Universidad de Santiago de Compostela, E-15706 Santiago de Compostela, Spain*

³*IPN Orsay/IN2P3, F-91406 Orsay Cedex, France*

⁴*DAPNIA/SPhN CEA/Saclay, F-91191 Gif sur Yvette Cedex, France*

⁵*CEN Bordeaux-Gradignan, F-33175 Gradignan Cedex, France*

(Received 17 August 2005; published 25 January 2006)

The production of light and intermediate-mass nuclides formed in the reaction $^1\text{H} + ^{238}\text{U}$ at 1 GeV was measured at the Fragment Separator at GSI, Darmstadt. The experiment was performed in inverse kinematics, by shooting a 1 A GeV ^{238}U beam on a thin liquid-hydrogen target. A total of 254 isotopes of all elements in the range $7 \leq Z \leq 37$ were unambiguously identified, and the velocity distributions of the produced nuclides were determined with high precision. The results show that the nuclides are produced in a very asymmetric binary decay of heavy nuclei originating from the spallation of uranium. All the features of the produced nuclides merge with the characteristics of the fission products as their mass increases.

DOI: [10.1103/PhysRevC.73.014607](https://doi.org/10.1103/PhysRevC.73.014607)

PACS number(s): 24.75.+i, 25.40.Sc, 25.85.Ge

I. INTRODUCTION

In 1996, at GSI, Darmstadt, a European Collaboration started a dedicated experimental program, devoted to reaching full comprehension of proton-induced spallation reactions. Accurate knowledge of proton-induced spallation reactions is relevant both for fundamental research and for technical applications. Among the latter, the design of accelerator-driven systems (ADS) and radioactive ion-beam (RIB) facilities relies strongly on knowledge of the formation cross sections of residual nuclei produced in such reactions. This information is needed to calculate the short-term and long-term radioactivity building up in these facilities and thus is crucial for designing the shielding and estimating the residual activation of such devices. In ISOL-type radioactive ion-beam facilities, the formation cross sections are decisive in determining which nuclides far from stability can become accessible and for estimating the attainable secondary-beam intensities, once appropriate extraction and ionization procedures have been developed. Here, fission is of special interest, because it seems to be best suited for approaching the neutron drip line in the medium-mass range. An energy of 1 GeV/nucleon is estimated to be optimum for both applications [1,2].

In the past, the available experimental data on spallation reactions were scarce and fragmentary, and the predictive power of the computational codes traditionally used for the design and shielding of nuclear facilities was in most cases rather poor [3]. For this reason, a project devoted to studying, understanding, and modeling these nuclear reactions at energies around 1 GeV per nucleon started at GSI nine years ago. Within this project, the first comprehensive survey on nuclide production cross sections in $^{197}\text{Au} + ^1\text{H}$ [4,5] and $^{208}\text{Pb} + ^1\text{H}$ [6–8] at around 1 GeV per nucleon was made. Experiments on other systems or at other energies (in the range 0.3–1.5 GeV per nucleon) have been published or are still being analyzed ($^{208}\text{Pb} + ^1\text{H}$ [9,10], $^{238}\text{U} + ^1\text{H}$ [11–15], $^{56}\text{Fe} + ^1\text{H}$

[16,17], and $^{136}\text{Xe} + ^1\text{H}$ [17]). The essential goal of this project is the measurement of the formation cross sections of residual nuclei in a few key nuclear reactions. From nuclear-reaction theory and from phenomenological observations it is expected that the cross sections for proton-induced reactions above some tens of MeV behave smoothly with target mass and projectile energy. Therefore, three nuclides— ^{56}Fe , ^{208}Pb , and ^{238}U —which represent a typical construction material, a target material of the spallation neutron source, and a highly fissile nucleus, respectively, were chosen as the key nuclei to be investigated.

The study of light-residue production (from $Z = 7$ to $Z = 37$) in hydrogen-induced reactions of ^{238}U at 1 GeV presented here belongs to this systematic study. Together with other measurements, performed in the same experiment, which were dedicated to the formation of heavier residues by fission (from $Z = 28$ to $Z = 73$ [12,13]) and by spallation-evaporation (from $Z = 74$ to $Z = 92$ [11]) in the system $^{238}\text{U} + \text{hydrogen}$, the whole chart of the nuclides from $Z = 7$ was covered. The experiment was subdivided into different measurement regimes because different experimental techniques and analysis methods were applied in these different mass regions. For example, the heaviest residues could only be identified by the use of a thick energy degrader in the intermediate image plane of the fragment separator [18]. Special conditions were also met in the present work, since a very large range in magnetic rigidity had to be covered for investigating the light fragments. Along with the formation cross-sections, the longitudinal momenta of the fragments after the reaction were also measured. They provide information on the reaction mechanism and are used for revealing the binary (or fission-like) character of the decay owing to the Coulomb repulsion between the two fragments. Knowledge of the reaction mechanism is of great importance for the design of RIB facilities and ADS, and in general for the new generation

of accelerators at high intensities [19], because the radiation damage to the structures depends on the kinetic energy of the fragments. An overview of all the results for the reaction ^{238}U on hydrogen at 1 A GeV is given in a dedicated letter [20].

In the context of the production of exotic nuclei, it should be mentioned that 253 very neutron rich light reaction products in the range $9 \leq Z \leq 46$ from the interaction of ^{238}U projectiles with beryllium and lead targets were observed in a previous experiment [21] in the course of an experimental program dedicated to produce new neutron-rich isotopes [22], in particular ^{78}Ni [23], by using the same installations as the present experiment. In contrast, the present experiment emphasizes the reaction aspect and focuses on a systematic overview of the most strongly produced isotopes of the light elements in the system $^{238}\text{U} + ^1\text{H}$.

Apart from the technical applications, the measurement of formation cross sections is also of interest for fundamental research. In astrophysics, for instance, these cross sections enter into the description of the processes that affect the composition of energetic nuclei during their transport through the Galaxy from their source to the Earth where they are observed. Models for the propagation of cosmic rays rely heavily on knowledge of the formation cross sections of light nuclei from interactions of heavy nuclei in the interstellar medium [24], which mostly consists of hydrogen. Also, the study of the reaction mechanisms responsible for the production of the light nuclides is of great physical interest. In the reaction $^{238}\text{U} + \text{hydrogen}$ at 1 A GeV, apart from spallation reactions, which produce rather heavy fragments (at $Z \geq 75$, see Ref. [11]), most part of the cross section of the medium-mass residues results from fission reactions ([12,25–28]). One of the most important signatures of fission is the binary nature of the decay process. The light residues investigated in this work also showed a binary nature, but binary decay can occur also in multifragmentation-type processes [29]. The possible scenarios behind fission and multifragmentation are indeed strongly different, because the first presupposes the slow decay of a compound nucleus, whereas the second entails passage through a fast breakup phase. It has been discussed, whether the yield of such binary products [30] and the longitudinal momentum transferred to the decaying nucleus [31] can carry information on the reaction mechanism that produced them. In this work, we will discuss whether the light residues we observed are consistent with one or the other picture, making use of the two available observables, the velocities and the production cross sections of the residues.

II. EXPERIMENTAL TECHNIQUE

The experiment was performed in inverse kinematics at relativistic energy, that is, by shooting a 1 A GeV ^{238}U beam into a H_2 target. In these experimental conditions, the fragment escapes the target strongly focused in the forward direction and is detected in-flight prior to its β decay. Thus, the whole isotopic distribution can be obtained for every element, and the velocity of the identified nucleus can be precisely determined and used to deduce the reaction mechanism that generated that isotope. In this way, fission and fragmentation events can be

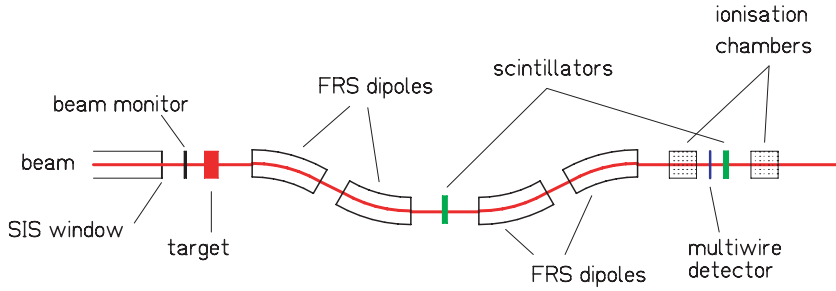
disentangled, as we will show. Another attractive peculiarity of this technique at around 1 A GeV is that the products are fully stripped and can be identified without any ambiguity caused by different charge states.

The SIS18 heavy-ion accelerator of GSI, Darmstadt, was used to provide the ^{238}U beam of 1 A GeV. The beam impinged on a liquid hydrogen target of 87.3 mg/cm^2 thickness, which was enclosed in a thin titanium casing [32]. A thin aluminum beam monitor was placed in front of the target. In the target and in the beam monitor, the primary beam loses a few percent of its energy; thus corrections from energy loss do not deteriorate the accurate measurement of the longitudinal momenta of the reaction residues. The reaction products entered into the fragment separator (FRS), which was used as a high-resolution spectrometer. The FRS [33] is a two-stage magnetic spectrometer, achromatic at the exit and dispersive in the central image plane. It has a momentum acceptance of 3% and an angular acceptance of 15 mrad around the beam axis. At the intermediate image plane, the fragments pass through a layer of matter (a scintillator, in our case). The energy loss of the fragments depends mostly on their charge. Every fragment will reduce its velocity and consequently its magnetic rigidity according to its atomic number. Owing to the limited momentum acceptance of the FRS, only a selected number of ions, with certain atomic numbers, will have adequate velocity to be transmitted along the second section of the FRS. This selection in Z forced us to divide the experiment into four measurements (this work, [11–13]), according to the transmitted fragments in the second section of the FRS. In the present work, only fragments with atomic number around $Z = 20$ could be transmitted. This limits the results between $Z = 7$ and $Z = 37$. The selection in Z turned out to be very useful for the measurement of light products. Their production cross sections are low compared to those of residues with higher mass and similar rigidity. In order not to overload the detectors, the intensity of the beam would have been limited by the high counting rate of the heavier fragments, and consequently the low counting rate of low-mass residues would have caused a large statistical error.

The essential detector equipment consisted of two scintillators, placed at the intermediate and final planes, and two ionization chambers, placed at the exit (see Fig. 1). Multiwire detectors placed in every image plane were used for beam monitoring and calibrations, but most of them were not in the beam line during the measurements.

The scintillation detectors were used to determine the time of flight of the fragments and their horizontal position (x position). The time of flight, together with the flight path, was used to deduce the velocity of the fragment. The x position gave the effective radii of the trajectory, which, multiplied by the value of the magnetic field, provided the magnetic rigidity of the fragment. Full identification of the reaction residues was performed by determining the atomic number Z from the energy-loss measurement with an ionization chamber, and the mass-to-charge ratio A/Z from the magnetic rigidity and the velocity, according to the equation

$$\frac{A}{Z} = \frac{e}{u} \frac{B\rho}{\beta_{\text{tof}}\gamma_{\text{tof}}c}, \quad (1)$$



where A is the mass number, Z is the atomic number, B is the magnetic field inside the magnet, ρ is the radius of the trajectory, u is the atomic mass unit, $-e$ is the electron charge, $\gamma_{\text{tof}} = 1/\sqrt{1 - \beta_{\text{tof}}^2}$ with $\beta_{\text{tof}} = v_{\text{tof}}/c$, where v_{tof} is the velocity of the ion, determined with the time-of-flight measurement, and c is the velocity of light. The energy-loss signal, ΔE , was corrected for the velocity dependence of the ion and for recombination losses. Since the nuclear charges of the fragments analyzed here are low and their velocity is high, practically all the fragments were completely stripped, and the ionic charges coincided with the nuclear charges without further corrections. The calibration of the atomic number of the products was performed by exploiting the parabolic dependence $\Delta E \propto Z^2$, whose minimum corresponds with $Z = 0$. In Fig. 2, the identification pattern for the nuclides analyzed in this work is presented. The pattern directly gave the mass calibration, thanks to the characteristic vertical line at $A/Z = 2$. An additional calibration of the atomic charge, independent from the previous one, was obtained by means of the identification pattern of Fig. 2. The inverse of the length of the generic horizontal line of Fig. 2, which represents the distance between two close isotopes, is represented by the following variable:

$$V = \frac{1}{[(A+1)/Z] - (A/Z)} = Z, \quad (2)$$

which directly gives the atomic number Z .

Once all reaction residues are identified, to every count filling the spectra of Fig. 2 one can associate an atomic number, Z , and a mass number, A . From this moment on, A and Z

are exact integer numbers with no associated error. In this way, the measurement of the magnetic rigidity $B\rho$ in the first half of the FRS, deduced from the horizontal position at the intermediate dispersive image plane, gives precise information on its longitudinal velocity v according to the equation

$$\beta\gamma c = B\rho \frac{e}{u + \delta u} \frac{Z}{A}, \quad (3)$$

where $\beta = v/c$ and $\gamma = 1/\sqrt{1 - \beta^2}$. In Eq. (3), δu is the mass excess per nucleon, which was neglected for the purpose of mass identification [Eq. (1)] but has to be taken into account here to provide a more precise result for the velocities. The magnetic fields are measured by Hall probes with a relative precision of 10^{-4} . The bending radius ρ is deduced from the position of the reaction products at the intermediate image plane with a relative uncertainty of about $\pm 2 \times 10^{-4}$, based on a resolution of $\text{FWHM} \approx 3$ mm in the measurement of the horizontal position. This results in an uncertainty of $\pm 2 \times 10^{-4}$ in the longitudinal momentum of individual reaction products.

Details of the experimental setup, in particular the fragment separator and the detector equipment [34,35], as well as a description of the analysis method [6,36,37] can be found in previous publications. Details of the experimental procedure and of the data analysis technique used in this work are documented in the underlying thesis [38].

III. DATA ANALYSIS

Because the limited momentum acceptance of the FRS of 3%, only part of the velocity spectra of a restricted

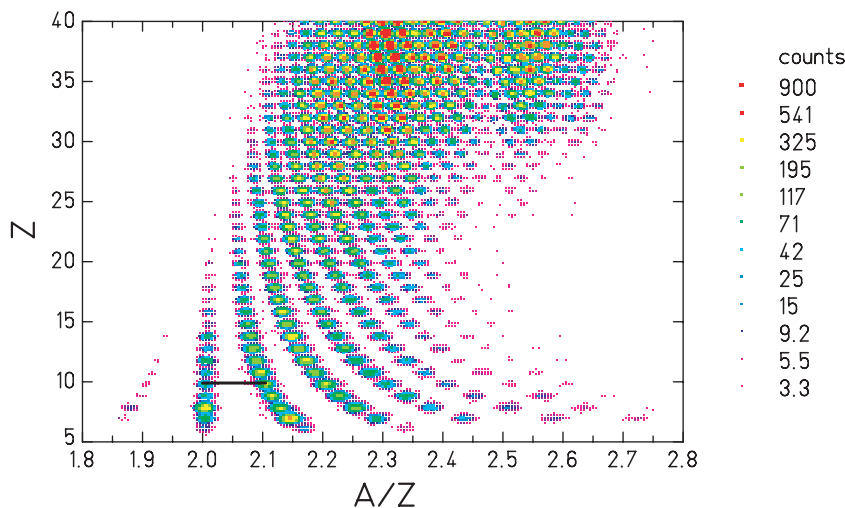


FIG. 2. (Color online) Identification pattern of the measured data. The vertical line at $A/Z = 2$ gives the mass calibration. The inverse of the length of the generic horizontal line, which represents the distance between two close isotopes, gives the atomic number Z (10 in the example) and provides the charge calibration. The plot collects the counts (given on a logarithmic scale) from the hydrogen target, including the contribution from the titanium windows of the container, for the present measurement (fragments with atomic number around $Z = 20$).

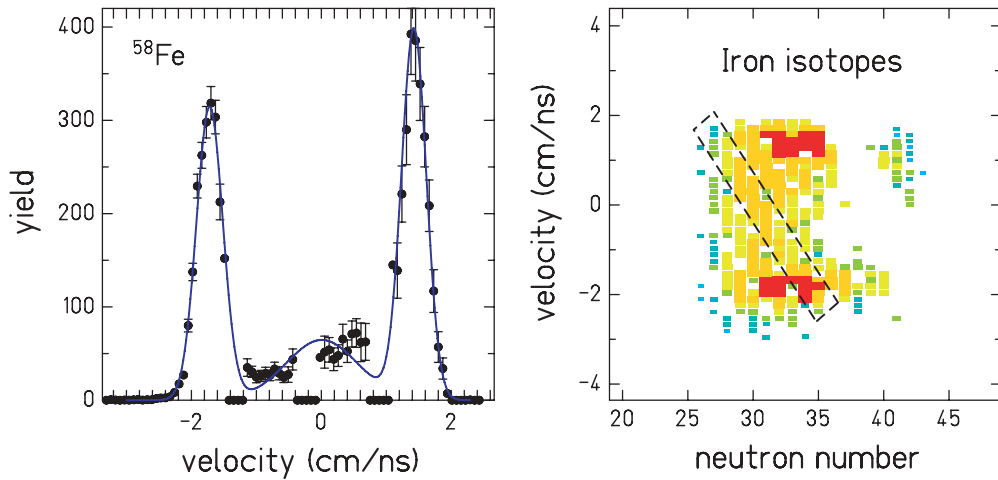


FIG. 3. (Color online) Left: Longitudinal-velocity spectrum for ^{58}Fe . The experimental data were fitted with three Gaussian curves. Right: Two-dimensional cluster plot of the velocity distribution as a function of the neutron number for iron ($Z = 26$). The dashed line encloses the events collected in one $B\rho$ measurement. In both figures, the data refer to the interaction of the uranium beam with $^1\text{H} + \text{Ti}$. The velocity is presented in the beam frame ($v_{238\text{U}} = 0$ cm/ns). The counts are normalized to the beam dose.

number of nuclides was measured at once. To fully cover the momentum distributions of all residues, measurements obtained by changing the magnetic fields in steps of 3% were combined. To do this, the spectra were normalized before to the number of beam-monitor counts and corrected for dead-time losses of the data acquisition. With this procedure, the longitudinal-velocity spectra were obtained for every observed nuclide. In Fig. 3 (left), the velocity distribution of ^{58}Fe in the beam frame is presented as an example. By combining the longitudinal-velocity spectra of all isotopes of one element, the two-dimensional cluster plot of the velocity distribution as a function of the neutron number was obtained for every element. In Fig. 3 (right), the cluster-plot velocity distribution of iron is presented as an example. One may notice that the counts are grouped into eight different transversal bands, for instance, the one enclosed inside the dashed line, corresponding to eight different $B\rho$ measurements. The missing band would contain products with the same magnetic rigidity as the beam, which could not be measured. The spectra in Fig. 3 include the contribution from the titanium windows of the container. An additional experiment, performed using a titanium target of the same thickness as the windows of the liquid-hydrogen container, provided the background production, which was subtracted to obtain the yield in hydrogen. From the data taken with the titanium target we deduced that the nuclei with the most extreme velocity values (covering the external wings of the velocity spectra in Fig. 3, left) are mostly due to the interaction of uranium with protons, whereas the central part is exclusively due to the interaction of uranium with titanium.

The spectra of Fig. 3 must be observed by keeping in mind that, owing to the limited angular acceptance of the FRS (15 mrad around 0°), represented by a cone in the laboratory frame, only the part of the production inside the cone is transmitted through the FRS and can actually be observed. According to what was found in previous experiments for similar systems [5–7,22,37,39–41], we assume that the situation can schematically be described as depicted in Fig. 4. The

three humps of the velocity distributions were interpreted as fission fragments emitted in the backward direction (left peak), fragmentation products (central peak), and fission fragments emitted in the forward direction (right peak). The interpretation was justified by the following considerations. The velocity distribution of the fragmentation residues is represented in the beam frame by a three-dimensional Gaussian [42]. A Gaussian-like shape is the result of the statistical superposition of several momentum contributions in space, attributed to the momenta of abraded nucleons [43] and to the recoil of evaporated particles. In peripheral collisions, owing to the abrasion, the longitudinal mean value is expected to be slightly

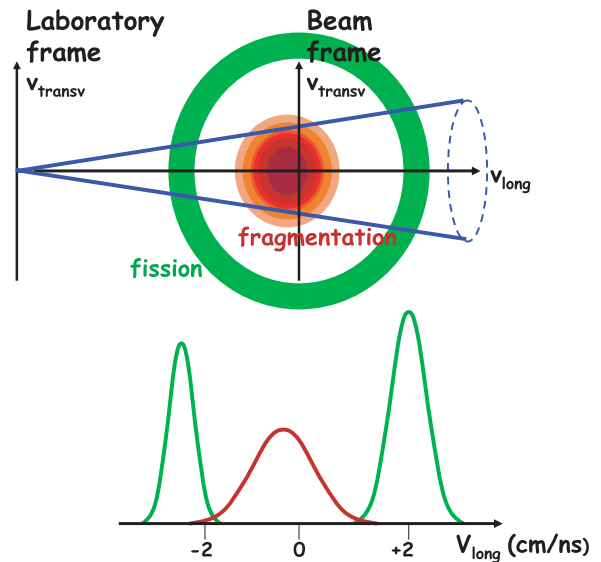


FIG. 4. (Color online) Top: Schematic representation of the velocity distributions of fragmentation and fission residues of one isotope, together with the FRS angular acceptance. Bottom: Projection of the accepted events on the longitudinal axis.

negative with respect to the beam velocity [44]. When the fragment is produced in a fission event, the kinetic energy that it acquires is more or less fixed, assuming that the fissioning nuclei belong to a limited range in Z and A , so the possible values of its velocity cover only the external shell of a sphere. The center of the sphere represents the mean velocity of the fissioning nucleus. In the beam frame it is slightly negative, because of the preceding abrasion or intranuclear-cascade process. The radius of this sphere results from the Coulomb repulsion between the fission fragments and momentum conservation, and thus it provides information on the mass and charge of the complementary fragment. This scenario also explains why the peak at positive velocities, corresponding to forward-emitted fission products, is higher than the peak of backward-emitted fragments, owing to the larger transmission of the FRS. Note that a similar pattern in velocity space can also result from other kinds of reactions such as evaporation of light fragments or breakup reactions with one heavy remnant. Keeping this remark in mind, in the following, for simplicity, we will call the reaction products showing this kind of kinematical pattern “fission fragments,” but we will return to a more general discussion later.

The interpretation of the data as fission and fragmentation products is consistent also with the characteristics of the isotopic distributions that could be extrapolated from Fig. 3 (right). The two peripheral humps (fission) are shifted to the right with respect to the central hump (fragmentation). As expected, fragmentation generally produces nuclei on the neutron-deficient side of the beta-stability valley, whereas in fission processes more neutron-rich fragments are produced. The velocity spectra observed inside the limited angular acceptance of the FRS turn out to be a useful tool to disentangle the different reaction mechanisms.

The shape of the velocity spectrum of every element was reconstructed by overlapping all the velocity distributions of the isotopes of that element. The overlapping was done by comparing channel by channel all the velocity distributions of the isotopes and taking the maximum value. This corresponds to overlapping the distributions of all the isotopes and drawing the skyline. In this way, every element contributes its most-produced fragmentation isotope and its most-produced isotope by fission processes to the velocity distribution. From a graphical point of view, this procedure corresponds to squeezing all the isotopes of the two-dimensional cluster plots of the velocity distributions, like the one of Fig. 3 (right), into one line. By combining the spectra of all the elements together, the two-dimensional cluster plot of the velocity distribution as a function of the produced elements could be constructed (Fig. 5). Figure 5 includes the contribution of the titanium windows, which is responsible for fragmentation products filling the central band of the distribution. The unexpected trend of the mean velocity of the fragmentation products, which increases with decreasing mass, is discussed in a separate publication [45].

The data analysis was based on the reconstruction of the full velocity distribution of each isotope. The extrapolation of the quantitative information from the raw spectra was not possible because some data were missing, as visible in Fig. 3 (right). A

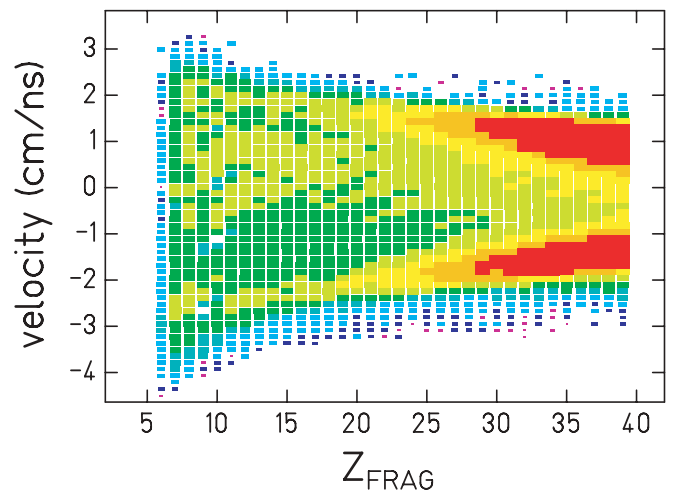


FIG. 5. (Color online) Two-dimensional cluster plot of the experimental velocities of fragments produced in the interaction of the uranium beam with the hydrogen-plus-titanium-window target. The velocity is presented in the beam frame ($v_{238\text{U}} = 0$ cm/ns).

fit with three Gaussian curves was used to reconstruct the full spectrum for every isotope (see Fig. 3, left). The procedure was optimized by fitting the data of every isotope on the basis of the results of a common fit obtained by fitting all the data at once, as explained in Ref. [38]. From the result of the fits, the mean values and the standard deviations of the longitudinal-velocity spectra and the yields inside the angular acceptance of the FRS could be determined for the fragmentation products and for fission fragments emitted in the backward and in forward directions.

The yields for the $^{238}\text{U} + ^1\text{H}$ system were deduced by subtracting the background yields obtained with the titanium dummy target. By assuming angular isotropy of the products, and using the method described in Ref. [46], the fraction of transmitted reaction residues can be calculated. Knowing the beam intensity, the target thickness, the angular efficiency of the FRS (“transmission ratios”) and the measured yields, the production cross-sections were obtained. An additional correction for the beam attenuation in the target was considered in the evaluation of the cross sections. The effect of secondary reactions in the target was in most cases negligible; however, the error bars were increased to account for this uncertainty. The contribution of secondary reactions was determined as described in the appendix of Ref. [6].

The finite angular acceptance of the spectrometer introduces a small deviation of the mean velocities and standard deviations from the true values. By assuming isotropic velocity distributions [9], these deviations were corrected using the transmission ratios. The mean velocity values were corrected also for the mean energy loss of the projectiles in the first half of the target and for the mean energy loss of the reaction products in the second half of the target. The average of the mean positions of the two peaks gives the mean recoil velocity of the mother nucleus in the beam frame introduced in the nuclear reaction. The mean value of the velocity of the fission fragments in the frame of the fissioning nuclei corresponds to the absolute value of the difference between

any mean positions of the two velocity peaks and the mean recoil velocity.

Below $Z=17$ the forward peak of the double-humped distribution could not be unambiguously determined owing to the contribution from the titanium target in this range. Therefore, the mean values of the velocity of the fission fragments are given only in the range $17 \leq Z \leq 39$. The backward hump was observable without discontinuity for $7 \leq Z \leq 39$. This fact permitted the fission cross sections for the entire Z range to be obtained by using the yield obtained from the fit of the backward hump. However, the results for $Z=38$ and $Z=39$ were excluded because they were at the extreme of the $B\rho$ selection, falling at the border of the scintillator at the exit of the FRS, with the consequence that part of the production could not be detected and their cross sections are systematically underestimated.

With the technique described here, the cross sections and the velocity distributions were measured for both reaction mechanisms (fission and fragmentation) for every nuclide produced in both systems ($^{238}\text{U} + ^1\text{H}$ and $^{238}\text{U} + \text{Ti}$).

IV. RESULTS

A. Measured production cross sections

In Fig. 6, the measured cross sections are presented in the form of isotopic distributions in the range $7 \leq Z \leq 37$. The numerical results are collected in Table A 1 of the Appendix. The statistical error was determined by the error associated to the fitted parameter in the individual fit of the velocity distribution of every nuclide. In turn, the latter reflects the statistical uncertainties associated with the single data points forming the velocity distribution, which were determined by the inverse of the square root of the number of counts, according to Poisson statistics. To account for the eventual deviations of the fit function from the “true” shape of the velocity distribution, the statistical uncertainty was increased until the square root of χ^2 divided by the degrees of freedom was approximately 1. Because of the asymmetry of the Poisson distribution, a confidence interval of 68% is not symmetric around the most probable value. This fact results in asymmetric error bars. This asymmetry is important for low counting and tends to disappear with a large number of events. The systematic uncertainties are due to the uncertainty on the width and mean value of the velocity distributions, the calibration factor that converts the beam-monitor counts into the number of ^{238}U projectiles, the evaluation of the angular transmission, the thickness of the target, and the secondary reactions. The production cross sections of some nuclides are missing, because the magnetic-field settings for those nuclei were not performed. In addition, some data had to be discarded for technical reasons. Those isotopes, for which the contribution of secondary reactions was estimated to be high, were also discharged.

The dashed lines in Fig. 6 were obtained with an interpolation by smoothing the existing data. When a data point is missing, the dashed line has to be taken just as a guideline for the eye. The dashed lines may not represent the real physical content, since the data do not necessarily follow a smooth

behavior, as explained in Ref. [47]. In Fig. 7, the cross sections for all the nuclides analyzed in this work are presented on the chart of the nuclides. As explained in the introduction, in the frame of the same experiment, three other works proceeded in parallel to analyze the data: In the fission region ($28 \leq Z \leq 64$ [12] and $65 \leq Z \leq 73$ [13]) and in the fragmentation region ($74 \leq Z \leq 92$ [11]). In this systematic study, the present work covers the part of the lightest nuclei ($7 \leq Z \leq 37$). In the region where two measurements overlapped (from $Z=28$ to $Z=37$) the experimental results generally agree within the error bars. The first, almost complete, general presentation on the preliminary data was discussed in Ref. [48]. The complete overview on residual-nuclide production cross sections is presented in Ref. [20] as a cluster plot superposed the chart of the nuclides. The numerical values for the entire set of data are available in Ref. [49]. It represents the most complete residual-nuclide distribution of a proton-induced spallation reaction on uranium ever obtained.

Regarding the region of light masses, three interesting aspects can be noticed from Fig. 6 and from the overview of Fig. 7. First, the isotopic distributions are long and shifted toward the neutron-rich side for the heavier fragments; they shorten and move toward stability as the mass decreases. As a second interesting fact, we observed that the production extends down to very light fragments. Our measurement was technically limited to $Z \geq 7$, but the production seems to extend even farther down. A third feature is the height of the cross sections. As expected, the cross sections are very high in the main fission region and decrease rapidly from $Z=30$ to $Z=20$. But then they stay constant and finally slightly increase again below $Z=10$. A discussion of these features will be presented in Sec. VI B.

B. Velocity distributions

The velocity distributions of the fragments contain other valuable information on the nuclear-reaction aspects. Although small changes of the mean velocities and of the standard deviations in the isotopic chain of one element are expected, the results will be presented as a function of the atomic number of the nuclides because no variation was observed inside the error bars among isotopes of the same element. The mean velocity of the fragments, presented in the frame of the mother nucleus, is shown in Fig. 8 (bottom). The mean recoil velocity of the mean mother nucleus in the beam frame is shown in Fig. 8 (top). Both figures also include the data obtained in the complementary analysis centered on symmetric fission [12]. As already stated, the data stop at $Z=17$ because the forward peak was not clearly disentangled below $Z=17$. In both figures, the error bars that are not visible are smaller than the data points. Numerical values are collected in Table A 2 of the Appendix. Table A 2 also collects the numerical values of the kinetic energies deduced from the data of Fig. 8.

In Fig. 9, we present the standard deviations of the two peaks of the velocity distributions of the fragments observed in forward and backward directions for $Z \geq 17$. The widths of the two peaks of the velocity distributions of the lighter nuclei in the backward direction with $Z < 17$ could not be determined with good precision, mostly because of the relatively large

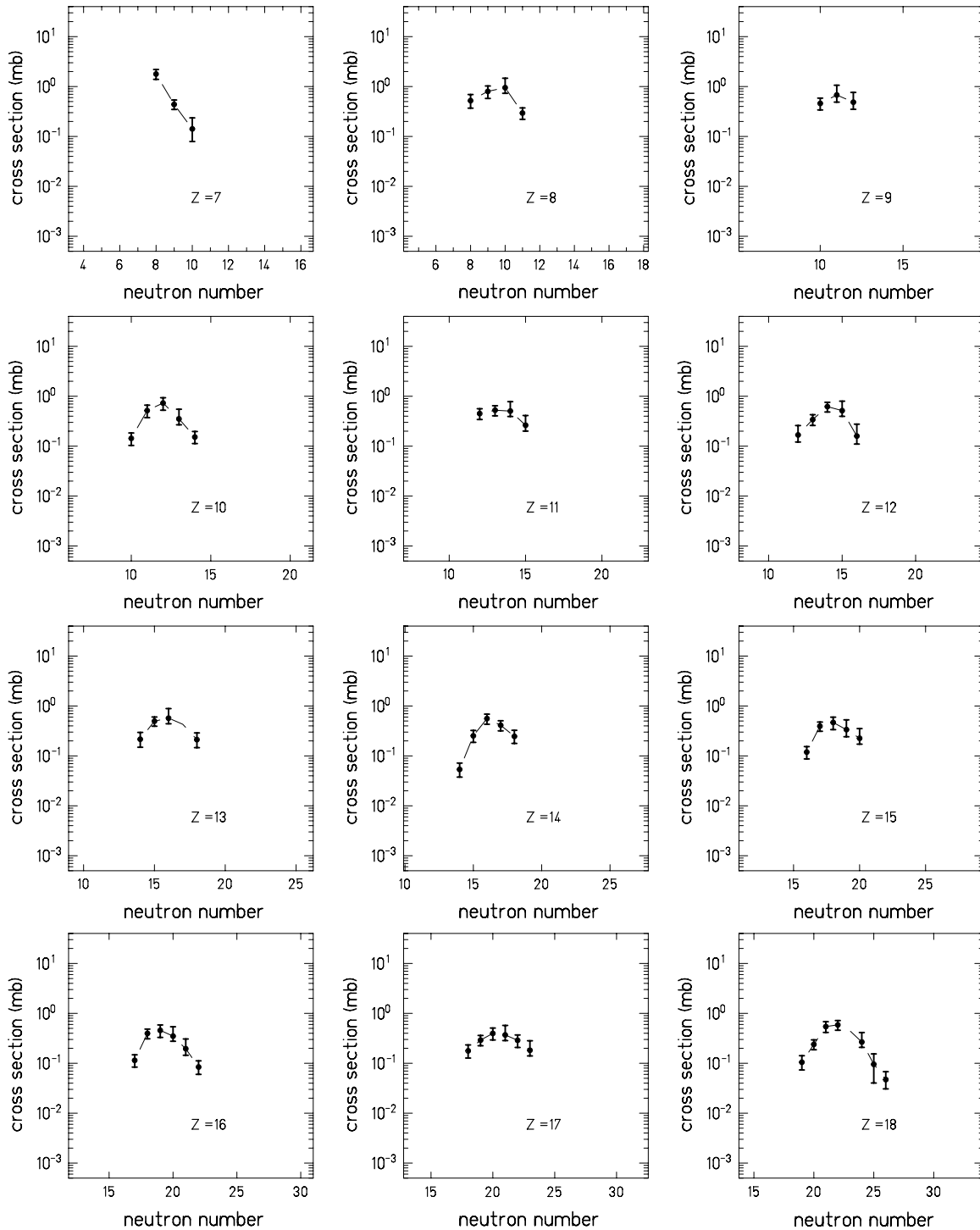


FIG. 6. Isotopic cross sections for the products between $Z = 7$ and $Z = 37$ produced in the reaction $^{238}\text{U} + ^1\text{H}$ at 1 GeV per nucleon. The dashed lines are set to guide the eye and do not necessarily represent the expected trend of the missing data. The error bars include both statistical and systematic uncertainties.

correction for the production in the titanium windows. These data do not give direct information on the physics of the reaction, since the widths of these distributions are affected by two main disturbing contributions. One is the finite angular range accepted by the FRS, which introduces an increase

in width in the longitudinal momentum (see Fig. 4). This contribution is larger for higher nuclear charges [46], which are transmitted more than the lower ones. The difference in energy loss of projectile and fragments in the target before and after the reaction introduces another energy broadening of

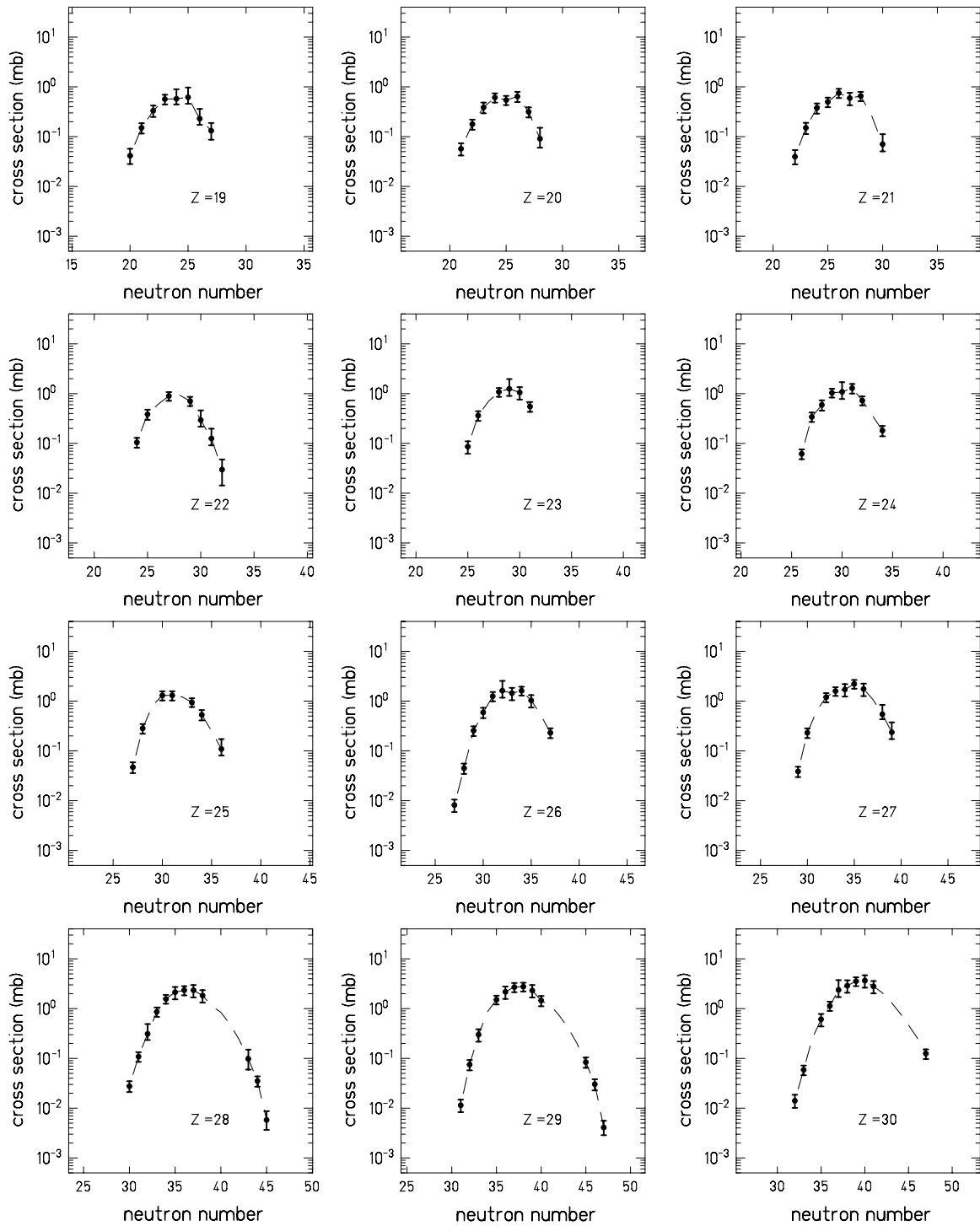


FIG. 6. (Continued.)

the residues, named “location straggling” [50], which slightly decreases with increasing nuclear charge. Both effects depend dominantly on the atomic number Z . In Table I, the measured widths of the backward velocity humps have been corrected for these two contributions for two nuclei, Ar and Sr. (In the calculation two isotopes were used.) The energy loss was

calculated with the program AMADEUS [51] and the effect of transmission was estimated as explained in Ref. [46]. For a specific nuclide, the relative width in velocity induced in the reaction $(\sigma_v^{\text{react}}/\nu)$ results to about 9–10%, approximately constant over the whole range of elements. This corresponds to a relative width in kinetic energy of the fragments of

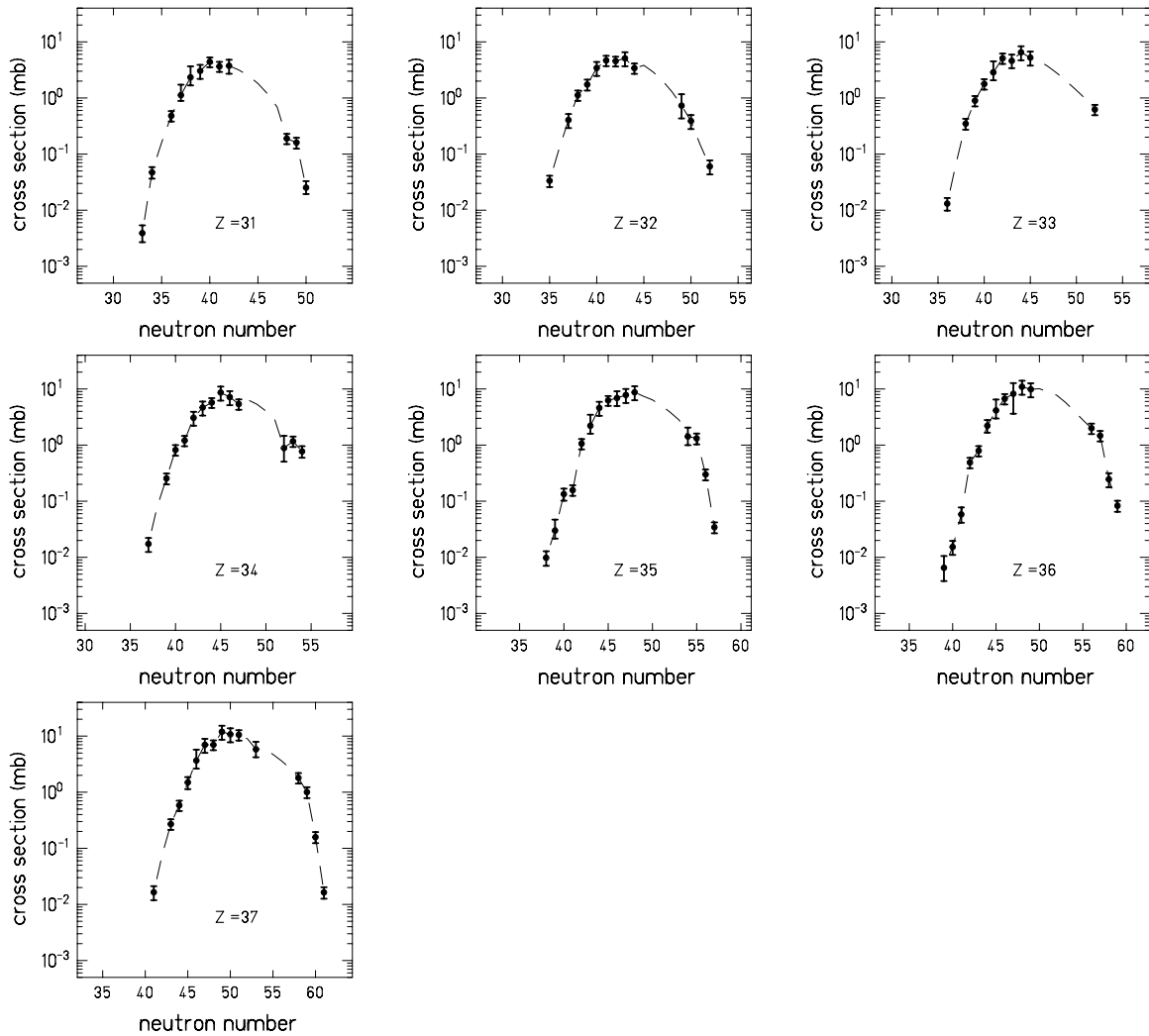


FIG. 6. (Continued.)

about 18–20%. For the heavier fission products ($Z \geq 30$), the absolute velocity width σ_v^{react} remains constant at about 0.125 cm/ns [12].

The values of σ_v^{react} include three contributions that cannot be disentangled from the present experiment. The first one emerges from the variation of the total kinetic energy (TKE) for a given fissioning system. The second is caused by the different fissioning systems contributing to the production of a certain fission fragment. The third one is caused by the

fluctuations of the velocity of the prefragment owing to the Fermi momenta of the removed nucleons. These latter aspects will be discussed also in Sec. VI C.

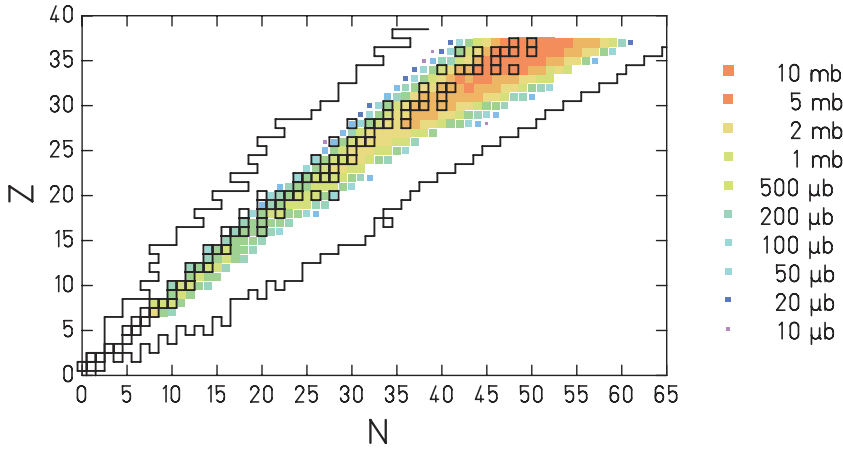
V. COMPARISON WITH OTHER DATA

A. Nuclide production

Data on the production of nuclides by nuclear fission, fully identified in Z and A , are scarce. Before the use of inverse

TABLE I. Contributions to the measured width σ_v^{meas} of the backward peak of the velocity distribution of two fragments from location straggling ($\sigma_v^{\Delta E}$) and from the variation of the longitudinal velocity in the transmitted angular range (σ_v^T). The velocity width caused by the nuclear reaction σ_v^{react} is deduced from the quadratic subtraction of the two terms. Combining the results for σ_v^{react} with those of Table A 2 one obtains the relative velocity width and the relative kinetic energy width (last two columns).

	σ_v^{meas} (cm/ns)	$\sigma_v^{\Delta E}$ (cm/ns)	σ_v^T (cm/ns)	σ_v^{react} (cm/ns)	$\frac{\sigma_v^{\text{react}}}{v}$ (%)	$\frac{\sigma_E^{\text{react}}}{E}$ (%)
^{40}Ar ($Z = 18$)	0.21	0.062	0.092	0.18	9	18
^{90}Sr ($Z = 38$)	0.19	0.045	0.118	0.14	10	20



- 10 mb
- 5 mb
- 2 mb
- 1 mb
- 500 μb
- 200 μb
- 100 μb
- 50 μb
- 20 μb
- 10 μb

FIG. 7. (Color online) Two-dimensional cluster plot of the nuclide production cross sections in the reaction $^{238}\text{U} + ^1\text{H}$ at 1 A GeV obtained in this work superposed on a chart of the nuclides. The numerical values of the measured data are collected in Table A 1. For those nuclides, that could not be measured, the cross sections were interpolated from the existing data by smoothing the isotopic distributions. The open black squares correspond to stable nuclides. The lines indicate the limit of the known nuclides.

kinematics, the measurement of the formation cross sections of individual nuclides mostly relied on their radiochemical properties and on the online mass-separator technique. In most counter experiments only mass distributions are obtained. In a recent experiment with secondary beams numerous element distributions have been determined [52]; however, no mass identification could be given. Only a few experiments on thermal-neutron-induced fission, performed at ILL, Grenoble, have given a rather comprehensive overview on nuclide production in the light fission-fragment group for a few odd- N fissile systems [53], but not extending below $Z \approx 26$ [54].

Data of excellent quality on nuclide production from higher excitation energies only exist for fission induced by relativistic ^{238}U projectiles in various targets (e.g. [37,41]), but they did not extend to very light elements.

For these reasons, very few experimental cross sections forming a full isotopic distribution comparable with our data are available. One of these few is that of rubidium ($Z=37$), measured by Belyaev *et al.* [55] in 1980. These data have already been compared with the results of the present experiment in Ref. [12], showing a good agreement. Yields of very light nuclides produced in interactions of 600-MeV protons with ^{238}U were already observed in direct kinematics [56]. As an example, in Fig. 10 the distribution of the potassium isotopes obtained in our experiment is compared to the yields measured at ISOLDE from 600-MeV protons in a thick uranium-carbide target [57]. The yields from the ISOLDE experiment (scale on the right) were normalized to our cross sections (scale on the left). The difference in energy is not expected to produce a significant difference in the cross sections [58]. The isotopic distribution is quite neutron rich with respect to the valley of beta stability. Since the ISOL

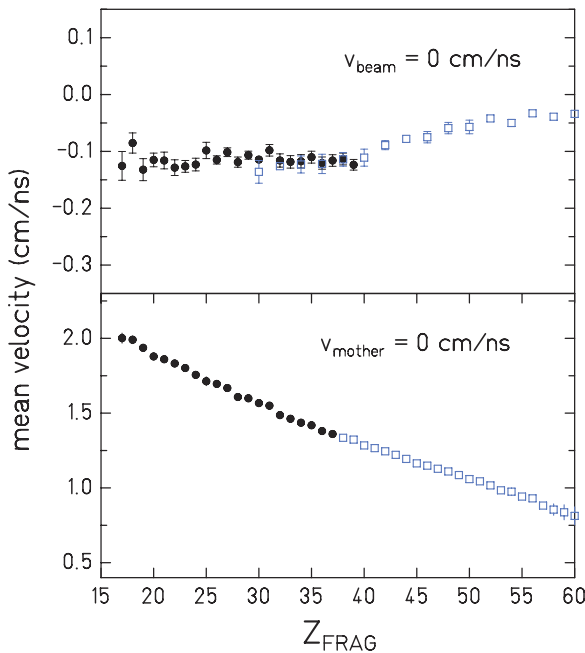


FIG. 8. (Color online) Experimental results for the reaction $^{238}\text{U} + ^1\text{H}$ at 1 A GeV. Top: Mean recoil velocities of the mother nuclei of all fragments measured in this experiment presented in the beam frame: this work (full dots), Ref. [12] (empty squares). Bottom: Mean values of the velocities of the fragments in the frame of the mother nuclei: This work (full dots), Ref. [12] (empty squares). Values are drawn as a function of the atomic number of the fragment.

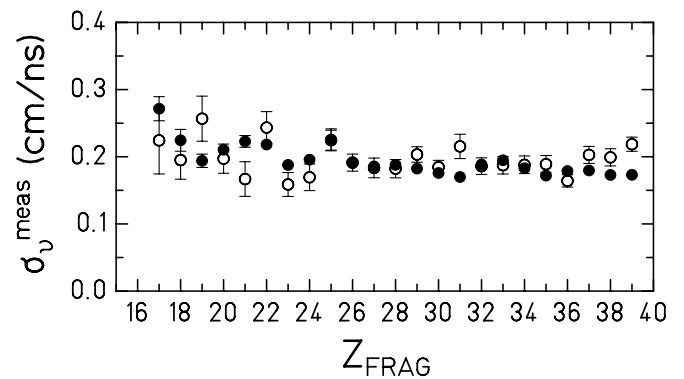


FIG. 9. Measured standard deviations σ_v^{meas} of the velocities of fragments emitted in the backward direction (full dots) and forward direction (empty dots), produced in the reaction $^{238}\text{U} + ^1\text{H}$ at 1 A GeV. The lines are the results given by the fitting procedure. The data are affected by the FRS angular transmission and by the location straggling in the target (see text). Values are drawn as a function of the atomic number of the fragment.

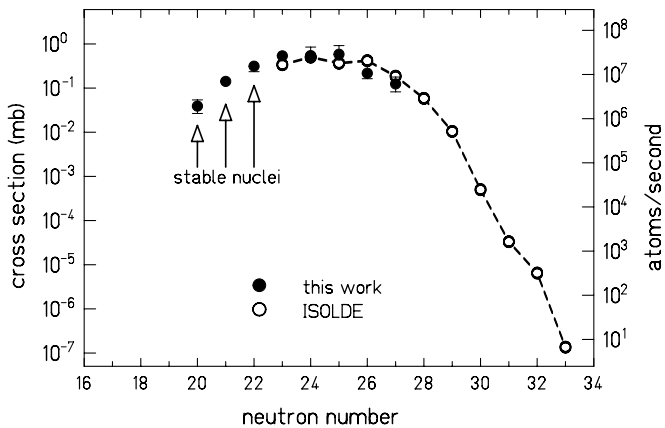


FIG. 10. Measured cross sections of potassium isotopes ($Z = 19$) from 1 A GeV ^{238}U in hydrogen of this work (full dots) compared with the yields of potassium isotopes from the reaction of 600-MeV protons in a thick uranium-carbide target (open dots), measured at ISOLDE [57]. The yields from the ISOLDE experiment (right scale) were normalized to the cross sections of this work (left scale).

method provides high efficiencies for a limited number of elements only, nothing can be learned about the overall nuclide production in the target from these measurements. Figure 7 can be considered a sort of “map” of the potentially available light radioactive beams by proton-induced reactions using a ^{238}U target. In addition, the systematic results offered by our measurements can be exploited for the determination of the efficiency of the ISOLDE technique.

The data of Ref. [57] were measured in direct kinematics. The experiments could not supply any information on the velocities; thus there was no knowledge on the reaction process that produced them. The velocity characteristics of the data measured in the present experiment indicate that the potassium isotopes presented in Fig. 6 formed in proton-induced spallation of ^{238}U at 1 A GeV originate from the binary decay of a heavy nucleus. We can deduce that the data of Ref. [57] also have the same kinematical characteristics.

In 1958 the production of ^{24}Na from proton-induced reactions on several targets at several energies was investigated [59]. The result for 1-GeV protons on ^{238}U can be compared with our data. The two measurements give (0.63 ± 0.16) mb [59] and (0.53 ± 0.12) mb [this work]. The results agree within the error bars.

B. Mass and charge distributions

A few additional rather dispersed data are available for yields of nuclides from reactions of protons with heavy nuclei. Most of them were measured with radiochemical detection methods in experiments performed in direct kinematics [60–65]. Only in a few cases, as for instance for 340-MeV protons on tantalum [66], does the mass distribution, deduced from the experimental data, extend with continuity from the heavy to the very light fragments, forming a W-shaped distribution (see Fig. 6 of Ref. [66]). In an experiment performed at LEAR (Low Energy Antiproton Ring) at CERN [67], the mass

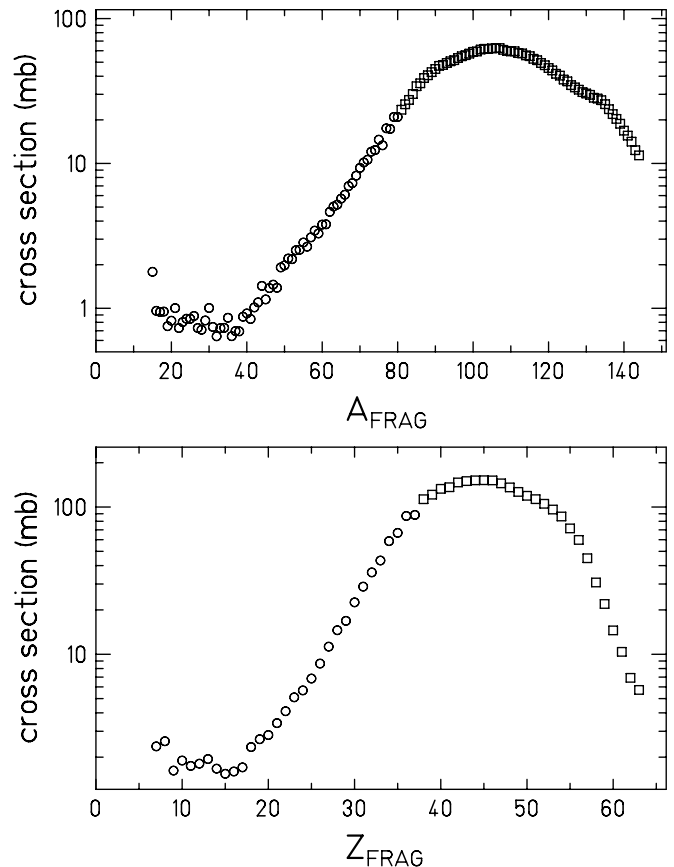


FIG. 11. Mass and charge distributions of binary-decay products measured in the reaction of $^{238}\text{U} + ^1\text{H}$ at 1 GeV. Dots: this work; squares: Taken from Ref. [12] in the range not covered by the present work.

distribution of fragments produced in the antiproton-induced fission of ^{238}U nuclei was obtained. The fission products could be selected by their kinetic energy and by a coincidence condition. The mass spectrum shows a minimum between $A \sim 20$ and $A \sim 40$ (see Fig. 2 of Ref. [67]). A similar behavior was also observed in the binary decay of a ^{244}Cm compound nucleus [68] produced in the heavy-ion fusion reaction of 8.4 A MeV ^{232}Th on ^{12}C (see Fig. 3 of Ref. [68]). The mass and charge distributions of the binary-decay products observed in this work also present a similar shape, as can be seen in Fig. 11, where the data are presented together with the other fission products measured in this experiment, analyzed in a separate work [12]. These results will be discussed in Sec. VI.

C. Velocities

In the review “Fission of highly excited nuclei,” Andronenko *et al.* [65] collected a large amount of experimental data for reactions induced by 1-GeV protons. Among other results, the review summarizes data on angular distributions, mean longitudinal momenta, and kinetic energies. Besides the review of Andronenko *et al.* such data are reported and discussed in

several publications (e.g. [25,69,70], and [31]). However, we could not find any measured data directly comparable with the light fragments produced in $^{238}\text{U} + ^1\text{H}$ at 1 A GeV, that were analyzed in this work.

VI. DISCUSSION

A. Possible reaction mechanism

In this section, the reaction mechanisms behind the production of light nuclides in spallation reactions will be discussed. In this context, it is useful to have an overview of the whole production, presented on the chart of the nuclides in Fig. 7 and in Ref. [20].

The proton-rich heavy evaporation residues, filling the upper part of the chart of the nuclides, are characterized by narrow, Gaussian velocity distributions, with mean values close to the velocity of the projectile. One may wonder whether the light fragments observed in the present work could be spallation-evaporation residues. Selecting cinematically the evaporation residues, Taïeb *et al.* [11] proved that the spallation-evaporation corridor in $^{238}\text{U} + ^1\text{H}$ at 1 A GeV dies out rather soon (around $Z = 74$).

As already discussed, owing to the angular cut of the FRS, the fission fragments are characterized by a double-humped distribution of the longitudinal velocity. The shorter is the distance between the two humps, the smaller is the velocity of the fragment [12]. This distance decreases as the charge of the fragment increases. At $Z > 63$, the two humps start to merge and form a single hump. Up to the last element investigated ($Z = 74$) the width of this hump is too large to be interpreted as the velocity spectra of just a spallation-evaporation residue. Thus the large width of the hump indicates a fission fragment and is consistent with the existence of a complementary light fission partner with large velocity, the fragments observed in the present work.

In a consistent way with what was observed in [12], the present experiment proves by the velocity distributions that the light nuclides in the spallation of ^{238}U by 1-GeV protons are produced together with a complementary heavy residue. Taking into account conservation of the momentum and the Coulomb repulsion between the light nuclide and its complementary heavy residue explains the large velocity in the beam frame. These velocities follow the pattern indicated by the heavier fission fragments (Fig. 8, bottom). Also, the charge and mass distributions of Fig. 11 do not present any discontinuity. All the experimental evidence indicates that the light residues observed in this work are fission fragments. As will be discussed in the next section, it is even expected from theoretical considerations and proven by several experiments (e.g. [67,68]) that mass distributions in fission show increased production yields for very asymmetric mass splits. These very asymmetric splits have been interpreted as a natural transition from fission to evaporation.

The fission-evaporation mechanism is certainly responsible for the production of light fragments. However, one may question whether this is the dominant production process. In the past, discussion [31] took place of whether the production of the light nuclides could be due mostly to a fast binary

decay right after the intranuclear cascade phase, before a fully thermalized compound nucleus is formed. Such a process would release residual nuclei having characteristics similar to those of the fragments observed in the present work: Large velocities (increasing as the mass decreases) and rapidly increasing cross sections with decreasing Z , below $Z = 10$.

In view of these considerations, we will discuss first the role of fission-evaporation in the production of the light residues (Sec. VI B). Then the contribution of a possible breakup channel will be discussed (Sec. VI C).

B. Fission

1. Transition from fission to evaporation

According to the transition-state model, the decay rate for fission depends on the properties of the fissioning nucleus in the “transition state,” that is, on the phase space available in the saddle-point configuration. The saddle point represents a kind of bottleneck through which the nucleus is forced to pass on the way to fission [71]. At the saddle point the potential energy U , associated with the shape (deformation ε) of the nucleus, $U(\varepsilon)$, has reached a maximum. The height in energy of this maximum with respect to the ground state of the nucleus is the fission barrier B_{fiss} . The potential energy depends also on mass-asymmetric deformations, which lead to the formation of two fragments of different sizes [72]. The relation between mass-asymmetry deformation at saddle and mass split at scission is assumed to be essentially strict and undisturbed by fluctuations resulting from the dynamics of the system between saddle and scission [73]. If A_1 and A_2 are the masses of the two fragments, the mass-asymmetric deformation can be expressed in terms of the “mass asymmetry parameter” $\eta = A_1/(A_1 + A_2)$. Consequently, the fission barrier can also be calculated for every mass asymmetry: $B_{\text{fiss}}(\eta)$. The potential energy forms a ridge line along the mass-asymmetry coordinate whose points are called “conditional saddle points” because of the constraint of a fixed mass asymmetry [73]. The energy of the conditional saddle points as a function of the mass asymmetry is illustrated in Fig. 12 for some nuclear systems. A description of the correlation of the final mass distribution and the variation of the height of the conditional saddle with mass asymmetry can be found in Ref. [74].

In the statistical model of fission [75,76], for a given excitation energy the yield of a certain fission fragment is calculated by the statistical weight of the transition states above the conditional potential barrier. This weight is in turn correlated to the density of nuclear levels. In the thermodynamic Fermi-gas picture) (i.e., assuming the nucleus as a system of noninteracting fermionic particles), the density of states is in good approximation given by

$$\rho(E_{\text{saddle}}^*) \propto e^{2\sqrt{aE_{\text{saddle}}^*}} \quad \text{with} \quad E_{\text{saddle}}^* = E_{\text{gs}}^* - B_{\text{fiss}}(\eta) \quad (4)$$

and $a \cong A/10 \text{ MeV}^{-1}$,

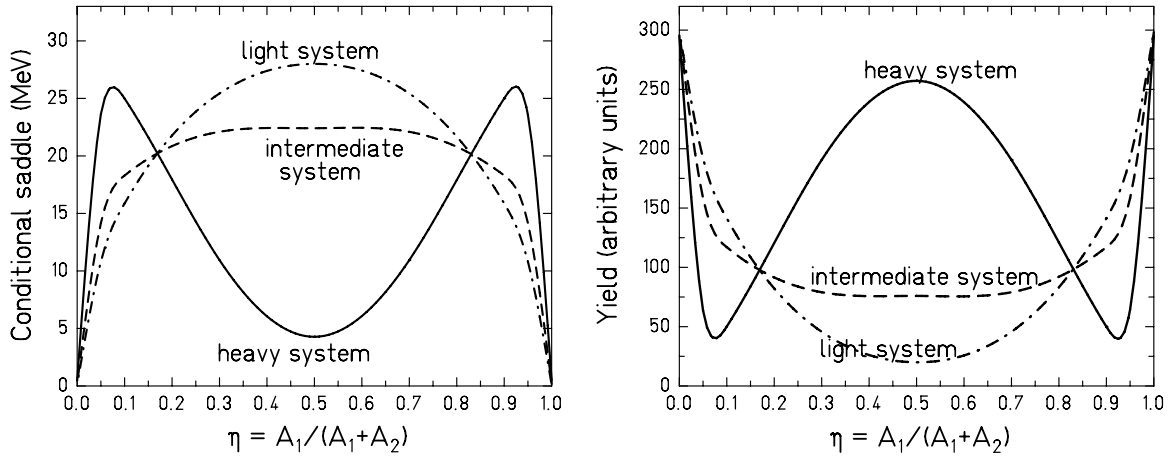


FIG. 12. Left: Schematic presentation of the fission-barrier height for a given mass split for light, intermediate, and heavy systems. Right: Corresponding yields (in arbitrary units).

where E_{gs}^* is the thermal excitation energy above the ground state and E_{saddle}^* is the energy above the saddle point. The yields as a function of mass asymmetry are then given by

$$Y(\eta, E_{\text{saddle}}^*) \propto e^{2\sqrt{a(E_{\text{gs}}^* - B_{\text{fiss}}(\eta))}}. \quad (5)$$

The result, for a heavy fissile nucleus at high excitation energies, is essentially a W-shaped distribution (see Fig. 12), whose maximum is at the symmetric split.

The central part of the M-shaped potential can, to a first approximation, be described by a parabola, whose curvature C_η affects the width of the central part of the mass distribution, which becomes a Gaussian function, with variance

$$\sigma^2(\eta, E_{\text{saddle}/\eta=1/2}^*) = \frac{1}{2} \sqrt{\frac{E_{\text{saddle}}^*}{a}} \frac{1}{C_{\eta=1/2}} = \frac{1}{2} \frac{T}{C_{\eta=1/2}} \quad (6)$$

with $T = \sqrt{E_{\text{saddle}}^*/a}$. The excitation energy introduced in the system and the curvature of the potential affect the width of the mass distribution. Therefore, in a heavy system, the difference in intensity from the top of the yield at symmetry (for $\eta = 0.5$ in Fig. 12, right) to the minimum (for $\eta = 0.08$ in Fig. 12, right) is very large at low excitation energies. As a consequence, most of the experimental observations available in the literature for fission seems to die out for atomic numbers below $Z \approx 28$. This is one of the reasons why the very light products (from $A = 1$ to $A \sim 20$) produced in high-energy nuclear reactions have been previously attributed to a kind of fragmentation process. For a long time, fission and evaporation were treated as separate processes. Moretto [76] and Swiatecki [77] pointed out and discussed the inconsistency of the two separate pictures. They proposed that, by looking at fission in a generalized sense, evaporation and fission can be treated as two manifestations of the same kind of binary decay with a continuous transition [78,79].

In the review ‘‘Fission of highly excited nuclei’’ by Andronenko *et al.* [65], the mass distributions show the characteristics expected from the general properties of fission barriers as a function of mass asymmetry [72], as illustrated by Fig. 12: Whereas for heavy fissioning systems at high

excitation energies one observes symmetric fission distributions, characterized by Gaussian distributions that are centered around half the mass of the mother nuclei, lighter systems show flat or even U-shaped distributions. Thus, these findings are compatible with a generalized fission process, according to the proposition of Moretto. Also, the mass distributions of Refs. [67,68] were attributed to high-energy fission, extending to very large mass asymmetry. Although in these two cases it was possible to verify the binary nature of the decay, for the mass distribution of Ref. [66] obtaining information on the kinematics was not possible and no interpretation was proposed at that time.

To conclude, in the decay of any excited fissile compound nucleus, the full mass range is expected to be populated by binary decay, understood as a generalization of evaporation and fission. Therefore, this process contributes to the production of light residues in the spallation reaction analyzed in this work. Whether or not the dominant production mechanism will be discussed in Sec. VI C.

2. The mean velocities

The quantitative reproduction of the mean velocity of the fission products is not an easy task, because several effects can affect the experimental results, such as, for instance, the eventual presence of a third fragment or dynamical effects such as a possible expansion of the system before splitting. However, we want to estimate the mean velocity of the fragments for two opposite scenarios, under some specific—but rather realistic—assumptions. The two scenarios are (1) the binary splitting of a deformed compound nucleus, investigated at the scission configuration, and (2) the binary splitting of an undeformed compound nucleus into two touching spheres.

For the first scenario we make use of the assumptions introduced in the statistical model of Wilkins *et al.* [80], where the total kinetic energy was considered to be determined basically by the Coulomb repulsion of the two fragments at the

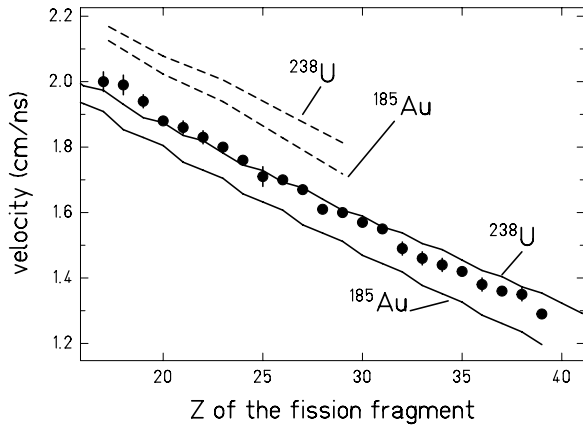


FIG. 13. Measured mean values of the velocities of fission fragments in the frame of the fissioning nucleus (\bullet). The lines represent the expected values of the velocity of fragments originating from the compound nuclei ^{238}U and ^{185}Au . The solid lines represent the expected velocities for the scission-point model (deformed nuclei) and the dashed lines the values obtained by the nucleus-nucleus fusion approach (undeformed nuclei).

scission point, whereas other terms were considered negligible (e.g., the energy from saddle to scission, which is mostly lost in dissipative phenomena). The mean velocity of the fission fragments is estimated by the following empirical liquid-drop description of the total kinetic energy:

$$TKE = \frac{Z_1 Z_2 e^2}{D} \quad \text{with} \quad D = r_0 A_1^{1/3} \left(1 + \frac{2\beta_1}{3}\right) + r_0 A_2^{1/3} \left(1 + \frac{2\beta_2}{3}\right) + d, \quad (7)$$

where A_1 , A_2 , Z_1 , and Z_2 denote the mass and atomic numbers of a pair of fission fragments prior to neutron evaporation; D represents the distance between the two charges and is given by the fragment radii ($r_0 A^{1/3}$), corrected for the deformation β plus the neck d . The parameters ($r_0 = 1.16$ fm, $d = 2.0$ fm, $\beta_1 = \beta_2 = 0.625$) were deduced from experimental data in ref. [81] and are consistent with values previously found in the analysis of Ref. [80]. Equation (7) is valid for sufficiently excited nuclei, where shell effects are negligible. When momentum conservation is imposed on the reaction, the velocities of the two fission fragments are determined. We have estimated the mean velocities of the fission fragments for two compound nuclei: $^{238}_{92}\text{U}$ and $^{185}_{79}\text{Au}$. They are compared with our data in Fig. 13. Whereas for the heavier fragments, the experimental data fall in between these two estimates, for fragments below $Z = 25$, the mean velocity tends to be higher than the estimation for the ^{238}U compound nucleus. This indicates that the experimental parameters of Eq. (7) that were obtained in symmetric fission are not applicable to very asymmetric mass splits. In very asymmetric fission, both the neck (parameter d) and the deformation (parameter β) seem to be smaller, with a consequent increase of the kinetic energy.

The opposite extreme of the situation described by Eq. (7) is the scenario of asymmetric binary decay from undeformed nuclei. In this context, we assumed that the binary decay can

be described as the inverse process of fusion. The shape of the potential is given in terms of the nuclear, Coulomb, and centrifugal contributions:

$$V_{\text{eff}} = -V_N + \frac{Z_1 Z_2 e^2}{r} + \frac{l(l+1)\hbar^2}{2\mu r^2}, \quad (8)$$

where Z_i are the charges, r is the distance between the centers of the nuclei, μ is the reduced mass, and l is the quantum number for angular momentum. In our calculations, the empirical nuclear potential of Bass [82,83] is used. The total kinetic energy of the two nuclei is assumed to be equal to the height of the fusion potential barrier. By imposing momentum conservation, the velocity of the two fragments was determined. The result of this calculation for the compound nuclei $^{238}_{92}\text{U}$ and $^{185}_{79}\text{Au}$ is represented in Fig. 13 by the dashed lines.

The comparison of the experimental data with the two set of calculations seems to indicate a tendency of going from a split into highly deformed nuclei to a split into undeformed nuclei as the charge of the fragments decreases. This result gives an indication that the lightest fragments are produced in configurations that are more compact than predicted by the systematics of Eq. (7) which is based on more symmetric fission.

The failure of the descriptions for the kinetic energies of very light fission fragments, which were deduced from symmetric fission of heavy systems (e.g. Ref. [84]) was already noticed and has led to some modified empirical formulations [20,85].

3. Comparison with the ABRABLA code

(a) *Charge and mass distributions.* In the charge and mass distributions of Fig. 11, the data show a clear deviation from a Gaussian shape at about $Z \approx 18$, $A \approx 40$.

In the following, we want to show that the observed change of slope of the distributions can be explained by means of the statistical model, by the binary decay of a fully equilibrated compound nucleus. To this purpose, we inserted the BURST model [86] in the statistical abrasion-ablation code ABRABLA [87–89], so that now spallation-ablation reactions can also be treated. Both codes were developed at GSI.

In the analytical code BURST, the prefragments arising from high-energy nucleon-nucleus collisions are calculated. The code is based on the parametrization of the output results of the intranuclear-cascade stage predicted by INCL3 [90]. It gives a consistent description of the numbers and the kinetic energies of protons and neutrons removed from the target and of the excitation energy and angular momentum acquired in the cascade of individual high-energy nucleon-nucleon collisions.

In the de-excitation stage of ABRABLA, named ABLA, the compound nucleus at every step of its evolution has two possible decay channels: evaporation and fission. Evaporation is treated as described in Ref. [88], the determination of the fission yields as described in Ref. [89], and the dynamical evolution of fission as described in Ref. [91]. In the statistical model of fission for a given excitation energy the yield of a certain fission fragment is determined by the statistical weight

of the transition states above the potential barrier (i.e., at the saddle point). This weight is in turn correlated to the density of nuclear levels. In ABLA, the latter are calculated using the thermodynamic Fermi-gas picture, that is, by assuming the nucleus to be a system of noninteracting fermionic particles. The potential energy at the saddle point depends on mass-asymmetric deformations, which lead to the formation of two fragments of different sizes. In the fission model of ABLA, the barrier as a function of mass asymmetry is defined by three components. The first is the symmetric component defined by the liquid-drop potential by means of a parabolic function with a curvature obtained from experimental data [92]. This parabola is modulated by two neutron shells, represented by Gaussian functions. Shells are supposed to wash out with excitation energy [93]. The heights and the widths of the Gaussians representing the shell effects and additional fluctuations in mass asymmetry acquired from saddle to scission are derived from experimental data [89]. This representation of the barrier as a function of mass asymmetry is valid only for the main fission region (from $Z \approx 20$ to $Z \approx 65$), whereas for very asymmetric mass splits the potential energy is expected to invert the slope and start to decrease, as discussed in Sec. VI B 1. Up to now, this approximation was considered sufficient since fission was expected to die out rapidly below $Z \sim 28$.

To correctly describe the binary decay of the compound nucleus also for very asymmetric mass splits one should properly model the M-shaped potential energy as a function of the mass asymmetry (Fig. 12, left). This is for instance the treatment applied in GEMINI [94]. We used another approach. In the previous section, we concluded that the lightest fragments are produced in a rather compact configuration. We take this evidence as an indication that there is gradual transition from the standard fission process toward evaporation. From the physical point of view an extremely asymmetric binary split into two compact nuclei corresponds to an evaporation of a light nucleus from a heavy compound nucleus. Up to now the evaporation part of ABLA considered only the emission of light particles, specifically, neutrons, protons, tritons, deuterons, ^3He , and alphas. In the code, we extended the evaporation to intermediate-mass fragments (IMF), that is, to the emission of light nuclei with $Z > 2$. The statistical weight for the emission of these fragments is calculated on the basis of the detailed balance principle. The decay width Γ as a function of the excitation energy E depends on the inverse cross section σ_{inv} , on the level densities of the two daughter nuclei, ρ_{imf} and ρ_{partner} , and on the level density of the mother nucleus above the ground state, ρ_C :

$$\Gamma \approx \int_0^{E_{\text{imf}}^{\text{max}}} \int_0^{E_{\text{partner}}^{\text{max}}} \sigma_{\text{inv}} \times \frac{\rho_{\text{imf}}(E_{\text{imf}}) \cdot \rho_{\text{partner}}(E_{\text{partner}})}{\rho_C(E)} (\varepsilon - B) dE_{\text{imf}} dE_{\text{partner}}, \quad (9)$$

with the following relation that guarantees energy conservation:

$$E = E_{\text{imf}} + E_{\text{partner}} + Q + \varepsilon - B. \quad (10)$$

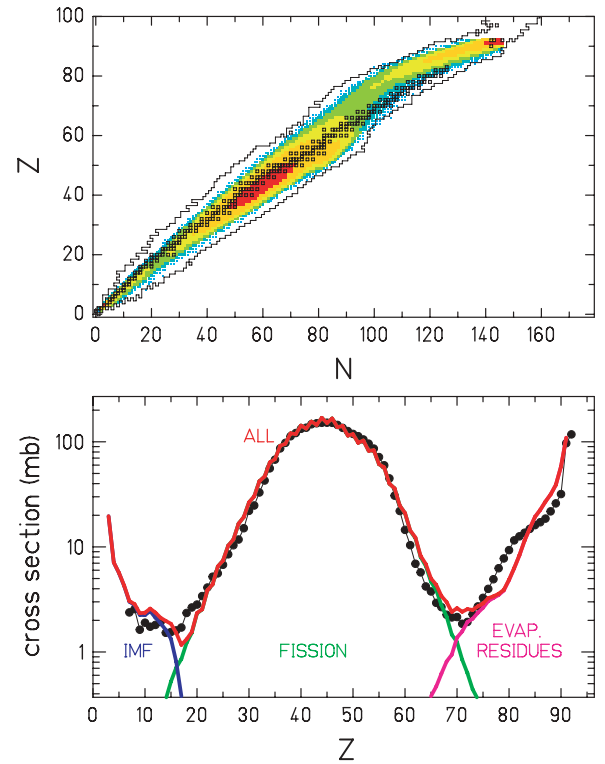


FIG. 14. (Color online) Cross sections for the nuclei produced in ^{238}U (1 A GeV) + ^1H . Top: Prediction of ABRABLA presented on the chart of the nuclides. Bottom: Experimental data (full dots) (this work, [11–13]) compared with the results of ABRABLA (solid line). The solid line is obtained by the sum of the three components: the evaporated IMF, the fission fragments, and the heavy evaporation residues (solid lines).

Here E , E_{imf} and E_{partner} represent the initial excitation energy of the mother nucleus and the excitation energies of the two daughter nuclei, respectively; Q is the Q value; ε is the total kinetic energy in the center-of-mass of the system; and B is the barrier of the potential. The barrier B was calculated by using the fusion nuclear potential of Bass [82,83]. The inverse cross section σ_{inv} was calculated by using the ingoing-wave boundary condition model [95], where only a real potential is used to describe the transmission probability of particles. An analytical approximation to Eq. (9) was used to avoid the numerical calculation of the two integrals, which is rather time consuming. This technical procedure will be described elsewhere.

One may object that, although the mean velocities of the fragments presented in Fig. 13 indicate that the two nuclei are formed in a rather compact configuration, they are not completely underformed. The deformation energy should be included for a consistent description. However, other effects, such as the thermal expansion of the excited nucleus, the surface effects on the level densities, and the preformation probabilities, can affect the decay width. They influence the result in different ways, some increasing and others decreasing the decay width. Considering the good agreement of our calculation with the experimental results (see Figs. 14–16), the global influence of all these contributions seems to be small.

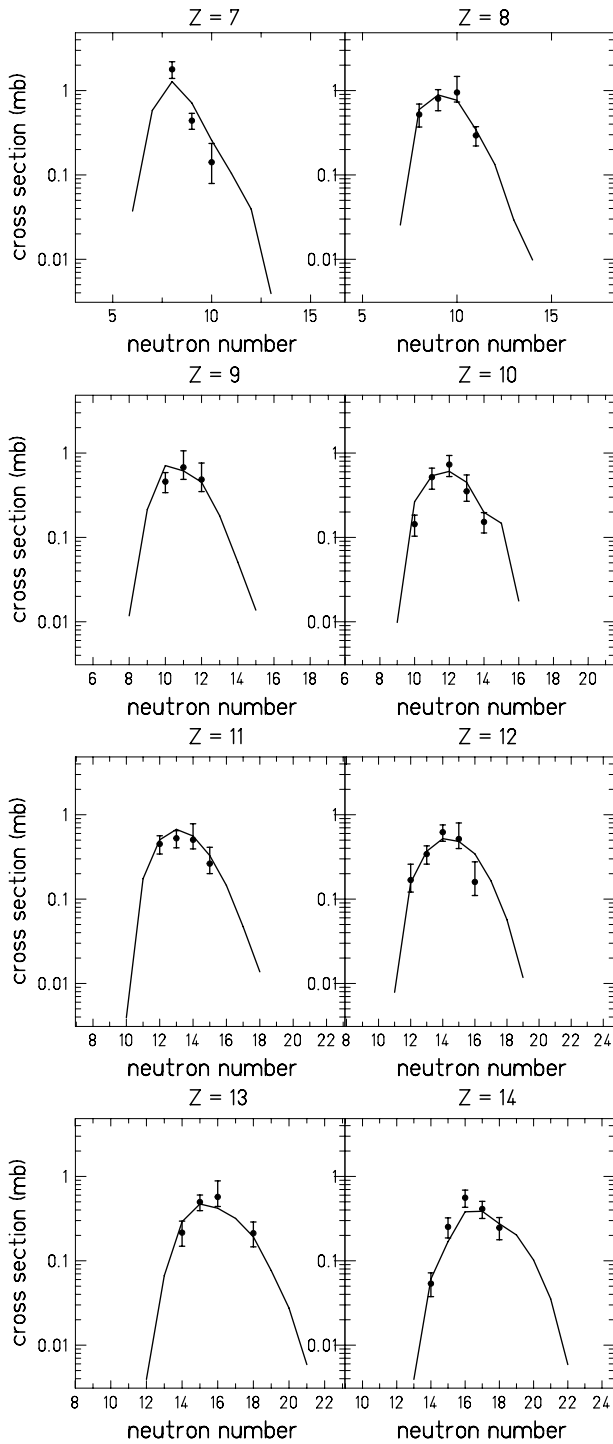


FIG. 15. Cross sections for the isotopes of the eight lightest elements measured in the reaction ^{238}U (1 A GeV) + p. The dots represent the experimental data measured in this work, the solid lines are the prediction of ABRABLA, which includes the evaporation of IMFs.

In Fig. 14, the result of the code is presented for the entire production range both on the chart of the nuclides (top panel) and as a charge distribution (bottom panel). The latter is compared with the experimental data. The figure includes the heavier fragments obtained in the parallel analysis [11–13]. We

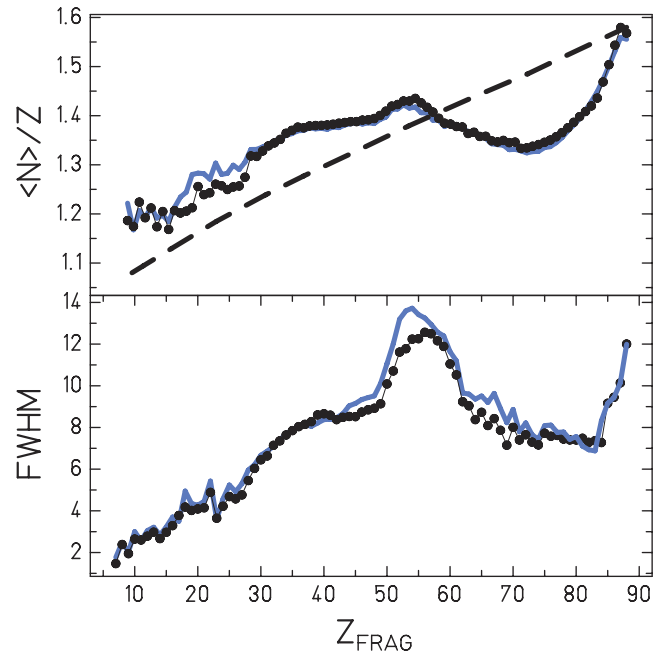


FIG. 16. (Color online) Top: Mean neutron-to-proton ratio of isotopic distributions as a function of the atomic number, compared with the stability line (dashed line) and to the ABRABLA prediction (solid line). Bottom: FWHM of the isotopic distributions compared to the prediction of the ABRABLA code (solid line).

recall that our measurement was technically limited to $Z \geq 7$, but the production of light nuclides would extend even farther down to $Z = 1$. The full line is obtained by the sum of the three components: the evaporated IMF, the fission fragments, and the heavy evaporation residues [although the evaporated light-charged particles ($Z \leq 2$) are also evaluated by the code, they are not included in the figure here]. In Fig. 15, eight isotopic distributions are compared with the calculation. In all the comparisons, the agreement is very good, proving that the binary decay of a fully equilibrated compound nucleus contributes in a dominant way to the production of light fragments.

We would like to point out that subdividing the description of the binary decay into two parts (IMF emission and standard fission) has the advantage of bypassing the description of the M-shaped conditional saddle, which is not an easy task. On the contrary, the semi-empirical approach used in ABLA has proven to be versatile and to have very good predictive power, especially for the description of low-energy fission, where the modeling of the fission channels plays a decisive role [89].

(b) *Mean value and width of the isotopic distributions.* In Fig. 16, the mean N/Z ratio and the standard deviations of the isotopic distributions are shown as a function of the atomic number for the entire production, which includes also the data of Refs. [11–13]. The dashed line represents the stable isotopes; the solid line is the result of the ABRABLA prediction.

In the fission model inside the ABLA code, the population of the fission channels is assumed to be basically determined by the statistical weight of transition states above the potential-energy landscape at the fission barrier, as described previously. Several properties, however, are finally determined at scission, among them the mean value and the fluctuations in the neutron-to-proton ratio, which are responsible for the so-called charge polarization [96]. The fluctuations in the neutron-to-proton ratio are considered by describing the potential in this degree of freedom with a parabolic function. By assuming that the equilibration in this variable is fast compared to the saddle-to-scission time, the curvature of this potential was calculated in a touching-sphere configuration. From knowledge of both the excitation energy and deformation energy of the system at the scission point, the excitation energies of the two fission prefragments can be sampled. The final fission fragments are then obtained at the end of the respective evaporation cascades. A full description of the model is given in Ref. [89].

Notice that the ABRABLA calculation reproduces correctly the mean values (the $\langle N \rangle / Z$ ratio) of the isotopic distributions. Also, the widths are well described, as can be seen in Fig. 16. This indicates that both the charge polarization in the fission process and the competition with the evaporation of nucleons in the statistical model are rather well described in the code.

The light products are neutron rich, as expected in fission. Compared to electromagnetic-induced fission (see, e.g., Refs. [37,39,40]), where the mean N/Z is closer to that of ^{238}U , here the neutron excess is lower, demonstrating that the process occurred at higher excitation energies. The neutron enrichment decreases slightly with decreasing mass, as well as with the width of the distribution. The latter effect is more evident. The reason for these tendencies is connected to the fact that the valley of stability becomes quickly narrow and steep. Large fluctuations in N/Z become more and more unlikely.

To conclude this section, we like to point out that the result of the ABRABLA code is remarkable, because the theoretical model behind it could never be compared with experimental results on fully identified nuclide distributions in the region of light fission fragments from proton-induced fission before. This is important, not only for the physics content, but also for the technical applications, where most of the available codes used to predict formation cross sections in fission reactions are based on empirical systematics (e.g. [97]), whose predictive power has proven to be rather poor [98].

4. Ternary fission

In the previous section we showed that all the experimental observables are consistent with the characteristics expected for fragments produced in binary fission. However, since only one particle was recorded in one event, one may question whether the observed light fragments could be produced in ternary fission [21]. In this context, it is useful to recall the results presented in Ref. [99], where the kinetic-energy distributions of Be and C fragments observed in coincidence

with fission fragments are presented. The light Be and C nuclei emitted at 50° with respect to the scission axis present Gaussian-like distributions peaked at around 43 and 53 MeV, respectively. However, when the light Be and C nuclei are observed at 90° , two additional Gaussian-like humps appear at 22 and 26 MeV for Be and C, respectively. The authors interpret these data assuming that the component at higher energy is associated with pre-scission emission events, which are essentially isotropic. These nuclei are presumably emitted in an earlier step of the de-excitation cascade preceding the fission process. The component at lower energy is due to ternary fission, that is, to light nuclei emerging from the neck of the system, traveling at about 90° with respect to the scission axis.

In the present experiment, the existence of a lower energy component would result in an additional concentric shell with smaller radius in the kinematical pattern schematically represented in Fig. 4 and, consequently, in fivefold humped velocity spectra. Such an additional lower energy hump was never observed in the velocity spectra of our data (see Fig. 5). Therefore, we conclude that the light nuclei presented here were not produced in ternary fission.

C. Fast breakup process

In the preceding sections we have investigated the contribution of fission. We have concluded that fission plays a major role in the production of light fragments. However, it may not be the only process responsible for the formation of light products. Here we want to discuss the possible contribution of a fast breakup process. With fast breakup we mean a multifragmentation-like reaction mechanism. The dynamical picture, thought to be behind it, is that of a *fast* thermal expansion right after the intranuclear cascade phase, with the formation of two clusters, successively driven apart by Coulomb repulsion. In contrast to this fast process, the fission-evaporation picture assumes the *slow* decay of a fully equilibrated compound nucleus. Observables, which could hint at one process or the other, are the time scale of the process, the multiplicity distribution of the products, the excitation energy of the decaying system, its momentum transfer, and the mean velocity of the fragments. In the following, we will analyze all these signatures. We will also critically investigate the justification of previously drawn conclusions in some other works that found indications for fast breakup processes in similar systems.

1. Multiplicity

In our experiment, the measurement of multiplicity was not possible. Very light fragments from lithium to argon were also investigated in 1-GeV proton-induced spallation of gold and some lighter nuclei [30]. It was observed that the probability for multiple IMF production ($Z \geq 3$) with a multiplicity ≥ 3 in the reaction $\text{Au} + {}^1\text{H}$ at 1 GeV is only 0.4% (i.e., almost all decays are binary). One may expect that in the system ${}^{238}\text{U} + {}^1\text{H}$ at 1 A GeV the percentage will be comparable,

since the energies introduced and the sizes of the two systems are rather similar.

2. Time scale

A recent theoretical work [100] investigates the compatibility of the measured properties of light fragmentation products with a binary sequential decay model. It is found that the experimental charge and energy distributions of the fragments produced in the spallation of gold by 8.1-GeV protons are well reproduced. Only the time scale, deduced from angular correlations of IMFs, is off by about a factor of 3. Unfortunately, the method of angular correlations of light fragments is not applicable for the appreciably lower projectile energy of 1 GeV used in the present work, since the probability for the emission of more than one light fragment is very low [101]. Eventual evidence on the compatibility with a fission process in the generalized sense might only be drawn from the other observables.

3. Excitation energy

In the reaction $\text{Au} + {}^1\text{H}$ at 1 GeV investigated in Ref. [30], along with the multiplicity equal to 2, the velocity spectra of the emitted light fragments indicate that they are produced by the binary decay of a heavy nucleus. Thus, the production of light fragments in this reaction is predominantly a binary process, forming one heavy and one light fragment. In Ref. [30], to deduce the excitation energy of the decaying system, the energy spectra were fitted with a Maxwellian distribution, with the assumption of isotropic emission. The deduced slope parameter gave an apparent temperature of about 8.4 MeV for all light fragments between $Z=7$ and $Z=18$. If interpreted as a temperature value, this would correspond to an excitation energy of about 1400 MeV in a fully thermalized system, which is even higher than the center-of-mass energy available in the reaction. However, in our opinion, the slope parameter cannot be interpreted as the temperature of the emitting source, because it is strongly influenced by several additional effects. One is the Fermi motion of the nucleons in a nucleus that is breaking up. This effect has been described by Goldhaber [43]. Its relevance for the interpretation of the kinetic properties of nuclear decay products has been underlined by Westfall *et al.* [70] and recently discussed in [102]. That means that the slope parameter of the energy spectra of the light fragments observed by [30] mostly reflects the velocity distribution of the nucleons in the decaying system and thus cannot be attributed to the characteristics of the decay process. There is also another effect, that has an important influence on the interpretation of the energy spectra. It relates to the fact that the light fragments may be produced by the decay of a variety of mother nuclei with different mass and atomic number. Also, this fact was not considered in [30]: This effect alone causes an important fluctuation of the kinetic energy of the emitted fragments. These two effects—the Fermi motion and the variety of emitting sources—make it rather difficult to find a straightforward quantitative interpretation of the slope parameter in terms of a “temperature parameter” in the energy

spectra of the IMFs produced in a 1-GeV proton-induced spallation reaction. We conclude that the large value of the slope parameter cannot be taken as proof for a fast binary decay occurring before the formation of a thermalized compound nucleus, as done in Ref. [30].

4. Momentum transfer

Barz *et al.* [31] reported folding-angle distributions of binary-decay products from the spallation of uranium, samarium, and silver by 1-GeV protons. Although for the binary-decay products of uranium the momentum transfer and its fluctuation are small, both quantities increase when going to samarium products. Fragments produced in the spallation of silver reveal a very large spread in momentum transfer, but no further increase of the momentum transfer. These findings were interpreted as an indication for the onset of multifragmentation in the lighter systems. As for the excitation energy, the very large spread in momentum transfer in the spallation of silver [31] can at least partly be related to the fact that the light fragments may be produced by the fission of a variety of mother nuclei with different mass and atomic number, without the need of introducing a multifragmentation process. Moreover, the Fermi motion of the abraded nucleons produces a similar effect. As discussed in Ref. [12], the same argument might also explain a great part of the rather broad relative kinetic energy width found in the present work (around 18% standard deviation; see Table I) when compared to the energy width known from low-energy fission of uranium isotopes, which amounts to only about 5% [103].

5. Mean velocities of the fragments

The mean velocity of the fragments with respect to the emitting source was the key information from which the binary nature of the decay was deduced. In Fig. 13 the comparison of the data with the results of calculations performed assuming a fission-evaporation scenario seems to reproduce satisfactorily the data. Under the hypothesis of a fast binary breakup, the expansion stage would result in a larger distance between the two clusters, with the consequence of a reduction of the Coulomb repulsion and eventually of the mean velocity. The possible presence of a third small cluster would sort out the same effect. In the end, we conclude that the mean velocities represent rather strong evidence that the reaction mechanism is a generalized fission process.

A similar investigation had been already performed in 1987 by Andronenko *et al.* [65]. He analyzed all the signatures (among which were angular correlations and mass and energy distributions) of the binary products from several proton-induced reactions at 1 GeV available at that time. The interaction of a proton with nuclei followed by fission, described by applying a cascade-evaporation model, could reproduce all the observed signatures, and he excluded the contribution of other decay modes. Similar conclusion were also drawn by Jahnke *et al.* [104] by studying the binary decay of uranium from the antiproton-induced reactions at 1 GeV. Also, Lott *et al.* [105] recently confirmed that binary products

of uranium from the antiproton-induced reactions at 1.22 GeV do not show any signature of multifragmentation.

We conclude that the results from several experiments, including the present work, give unanimous indications that light fragments in the reaction $^{238}\text{U} + ^1\text{H}$ at 1 A GeV are produced in a binary decay. Although the nature of this decay could not be identified without doubt, clear indications for a fast breakup process in this reaction seem to be absent. It may therefore be concluded that, at the current stage of knowledge, the experimental signatures in the reaction $^{238}\text{U} + ^1\text{H}$ at 1 A GeV are consistent with the binary decay of a fully equilibrated compound nucleus.

VII. CONCLUSIONS

Despite the long study of fission, there is still very little experimental information available on the light residues produced in the fission of actinides. Here, 254 light residues in the element range $7 \leq Z \leq 37$ formed in the proton-induced reactions of ^{238}U at 1 A GeV were presented. This experimental work belongs to a systematic study of the reaction $^{238}\text{U} + ^1\text{H}$ at 1 A GeV, where the production of nuclides with $7 \leq Z \leq 92$ was measured and analyzed. The other experimental data, complementing those presented here, can be found in Refs. [11–13].

The light fragments presented here, which populate the chart of the nuclides far down, could be qualified as binary-decay products owing to the available kinematical information. A detailed study of all the experimental observables—the mass and charge distributions, the isotopic distributions, and the mean velocities, the width of the velocity distributions, and the mean recoil velocities of the mean mother nuclei—showed that all these signatures are consistent with the binary decay of a fully equilibrated compound nucleus, whereas clear indications for fast breakup processes seem to be absent. As discussed in [78], the binary decay of a compound nucleus includes fission and evaporation with a natural transition in between, and it might be called fission in a generalized sense [73]. Thus, very asymmetric fission of the system $^{238}\text{U} + ^1\text{H}$ at 1 A GeV seems to reach down to rather light nuclei, extending below $Z = 7$ and merging with evaporation. In the spallation-fission reaction of ^{238}U this feature is unambiguously identified for the first time.

ACKNOWLEDGMENTS

We wish to thank F. Ameil, K. Günzert, and M. Pravikoff for their participation to the data taking, K. H. Behr, A. Brünle, and K. Burkard for their technical support during the experiment, and the group of P. Chesny for building and operating the liquid-hydrogen target. The work has been supported by the European Community with the programs “Human Capital and Mobility” under Contract No. ERBCHB-CT-94-0717, “Access to Research Infrastructure Action of the Improving Human Potential” under Contract No. HPRI-1999-CT-00001, “HINDAS” under the Contract No. FIKW-CT-2000-00031, and “EURISOL” under the Contract No. HPRI-1999-CT-50001.

APPENDIX

TABLE A1. Measured fission cross sections for the spallation of 1 A GeV ^{238}U on hydrogen.^a The last two columns represent the upper and lower relative uncertainties (expressed in percentage). Both statistical and systematic errors are considered. The cross section of those isotopes which either could not be measured or the measurement was rejected for technical reason (see text) are marked with the notation “==”.

Z	N	σ/mb	$\varepsilon_{\text{rel}}^{\text{up}}$	$\varepsilon_{\text{rel}}^{\text{dw}}$
7	8	1.8	23	22
7	9	0.44	22	21
7	10	0.14	67	44
8	8	0.52	33	29
8	9	0.8	28	28
8	10	0.95	55	23
8	11	0.29	27	25
9	10	0.46	28	26
9	11	0.68	57	28
9	12	0.49	57	28
10	10	0.14	28	28
10	11	0.52	28	28
10	12	0.73	28	28
10	13	0.36	56	24
10	14	0.15	29	26
11	12	0.45	25	24
11	13	0.53	23	23
11	14	0.5	55	22
11	15	0.26	56	24
12	12	0.17	54	28
12	13	0.34	25	24
12	14	0.62	22	22
12	15	0.52	55	23
12	16	0.16	73	31
13	14	0.22	37	31
13	15	0.5	21	21
13	16	0.57	55	23
13	17	==		
13	18	0.21	36	31
14	14	0.054	34	30
14	15	0.25	28	26
14	16	0.56	23	23
14	17	0.41	23	23
14	18	0.25	32	28
15	16	0.12	29	27
15	17	0.39	21	21
15	18	0.47	28	28
15	19	0.34	57	28
15	20	0.23	56	24
16	17	0.11	29	27
16	18	0.4	22	22

TABLE A1. (*Continued.*)

TABLE A1. (*Continued.*)

Z	N	σ/mb	$\epsilon_{\text{rel}}^{\text{up}}$	$\epsilon_{\text{rel}}^{\text{dw}}$	Z	N	σ/mb	$\epsilon_{\text{rel}}^{\text{up}}$	$\epsilon_{\text{rel}}^{\text{dw}}$
16	19	0.46	28	28	22	32	0.03	60	52
16	20	0.35	54	21					
16	21	0.2	57	26	23	25	0.086	28	28
16	22	0.084	33	29	23	26	0.36	22	22
					23	27	==		
17	18	0.18	32	28	23	28	1.1	20	20
17	19	0.29	24	23	23	29	1.3	57	28
17	20	0.4	28	26	23	30	1.1	28	28
17	21	0.37	55	23	23	31	0.55	23	22
17	22	0.29	28	28					
17	23	0.18	55	23	24	26	0.062	23	22
					24	27	0.34	22	21
18	19	0.11	35	30	24	28	0.59	24	23
18	20	0.24	23	22	24	29	1	20	20
18	21	0.55	25	24	24	30	1.1	57	28
18	22	0.59	22	22	24	31	1.3	22	22
18	23	==			24	32	0.73	21	20
18	24	0.27	55	22	24	33	==		
18	25	0.096	61	58	24	34	0.18	24	23
18	26	0.047	44	35					
					25	27	0.047	25	24
19	20	0.041	38	32	25	28	0.28	22	22
19	21	0.15	24	23	25	29	==		
19	22	0.33	27	25	25	30	1.3	21	21
19	23	0.57	22	22	25	31	1.3	21	21
19	24	0.58	56	23	25	32	==		
19	25	0.62	57	26	25	33	0.95	20	20
19	26	0.23	57	25	25	34	0.53	24	23
19	27	0.13	43	34	25	35	==		
					25	36	0.11	58	26
20	21	0.057	29	27					
20	22	0.18	23	23	26	27	0.0082	28	28
20	23	0.39	25	24	26	28	0.045	24	23
20	24	0.61	21	21	26	29	0.26	22	22
20	25	0.54	21	21	26	30	0.59	24	23
20	26	0.64	24	23	26	31	1.3	21	21
20	27	0.32	23	23	26	32	1.6	57	28
20	28	0.091	66	34	26	33	1.4	28	28
					26	34	1.6	20	20
21	25	0.5	22	22	26	35	1	28	28
21	26	0.76	21	21	26	36	==		
21	27	0.59	28	28	26	37	0.23	23	22
21	28	0.65	21	21					
21	29	==			27	29	0.039	24	23
21	30	0.07	59	28	27	30	0.23	22	22
21	22	0.04	36	30	27	31	==		
21	23	0.15	26	25	27	32	1.2	21	21
21	24	0.38	23	23	27	33	1.6	20	20
					27	34	1.7	28	28
22	24	0.11	23	22	27	35	2.2	20	20
22	25	0.39	24	23	27	36	1.8	28	28
22	26	==			27	37	==		
22	27	0.9	20	20	27	38	0.55	54	21
22	28	==			27	39	0.24	58	27
22	29	0.71	21	21	28	30	0.028	26	24
22	30	0.29	57	26	28	31	0.11	22	22
22	31	0.13	58	27	28	32	0.31	57	25

TABLE A1. (Continued.)

TABLE A1. (Continued.)

Z	N	σ/mb	$\epsilon_{\text{rel}}^{\text{up}}$	$\epsilon_{\text{rel}}^{\text{dw}}$	Z	N	σ/mb	$\epsilon_{\text{rel}}^{\text{up}}$	$\epsilon_{\text{rel}}^{\text{dw}}$
28	33	0.87	22	21	31	41	3.6	21	20
28	34	1.6	20	20	31	42	3.8	28	28
28	35	2.1	28	28	31	43	==		
28	36	2.3	21	21	31	44	==		
28	37	2.3	28	28	31	45	==		
28	38	1.8	28	28	31	46	==		
28	39	==			31	47	==		
28	40	==			31	48	0.19	21	21
28	41	==			31	49	0.16	22	22
28	42	==			31	50	0.025	31	23
28	43	0.01	54	39					
28	44	0.035	24	23	32	35	0.034	23	23
28	45	0.0058	50	37	32	36	==		
					32	37	0.41	28	28
29	31	0.011	30	27	32	38	1.1	21	21
29	32	0.075	24	23	32	39	1.7	22	22
29	33	0.3	28	28	32	40	3.4	28	28
29	34	==			32	41	4.7	21	21
29	35	1.5	20	20	32	42	4.5	20	20
29	36	2.2	28	28	32	43	5.1	28	28
29	37	2.7	21	21	32	44	3.4	21	21
29	38	2.8	20	20	32	45	==		
29	39	2.3	28	28	32	46	==		
29	40	1.4	24	23	32	47	==		
29	41	==			32	48	==		
29	42	==			32	49	0.73	59	41
29	43	==			32	50	0.39	28	28
29	44	==			32	51	==		
29	45	0.084	24	23	32	52	0.06	28	28
29	46	0.03	26	25					
29	47	0.0041	36	30	33	36	0.013	26	25
					33	37	==		
30	32	0.014	32	28	33	38	0.35	22	22
30	33	0.059	22	22	33	39	0.89	21	21
30	34	==			33	40	1.8	21	21
30	35	0.61	28	28	33	41	2.9	57	28
30	36	1.1	21	21	33	42	5.1	21	21
30	37	2.4	57	28	33	43	4.6	29	26
30	38	2.9	28	28	33	44	6.5	28	28
30	39	3.6	20	20	33	45	5.6	28	28
30	40	3.7	28	28	33	46	==		
30	41	2.8	28	28	33	47	==		
30	42	==			33	48	==		
30	43	==			33	49	==		
30	44	==			33	50	==		
30	45	==			33	51	==		
30	46	==			33	52	0.62	21	21
30	47	0.12	22	22					
					34	37	0.017	28	28
31	33	0.0039	38	31	34	38	==		
31	34	0.047	24	23	34	39	0.26	22	22
31	35	==			34	40	0.82	22	21
31	36	0.48	21	21	34	41	1.2	21	21
31	37	1.1	54	21	34	42	3.1	28	28
31	38	2.3	57	28	34	43	4.7	28	28
31	39	3	28	28	34	44	5.7	20	20
31	40	4.4	20	20	34	45	8.6	28	28

TABLE A1. (*Continued.*)

Z	N	σ/mb	$\varepsilon_{\text{rel}}^{\text{up}}$	$\varepsilon_{\text{rel}}^{\text{dw}}$
34	46	7.2	28	28
34	47	5.4	21	21
34	48	==		
34	49	==		
34	50	==		
34	51	==		
34	52	0.89	65	43
34	53	1.2	21	21
34	54	0.77	24	23
35	38	0.0098	31	28
35	39	0.03	57	28
35	40	0.13	25	24
35	41	0.16	22	21
35	42	1.1	21	21
35	43	2.2	57	28
35	44	4.6	28	28
35	45	6.3	20	20
35	46	6.9	32	28
35	47	7.8	28	28
35	48	8.8	28	28
35	49	==		
35	50	==		
35	51	==		
35	52	==		
35	53	==		
35	54	1.4	44	30
35	55	1.3	22	22
35	56	0.3	22	22
35	57	0.034	22	22
36	39	0.0065	62	42
36	40	0.015	28	28
36	41	0.058	33	29
36	42	0.49	21	21
36	43	0.79	21	21
36	44	2.2	26	25
36	45	4.1	57	28
36	46	6.7	21	21
36	47	8.2	55	56
36	48	11	28	28
36	49	10	28	28
36	50	==		
36	51	==		
36	52	==		
36	53	==		
36	54	==		
36	55	==		
36	56	2	21	21
36	57	1.5	21	21
36	58	0.25	28	28
36	59	0.083	23	22
37	41	0.017	28	28
37	42	==		
37	43	0.27	22	21
37	44	0.58	21	21

TABLE A1. (*Continued.*)

Z	N	σ/mb	$\varepsilon_{\text{rel}}^{\text{up}}$	$\varepsilon_{\text{rel}}^{\text{dw}}$
37	45	1.5	25	24
37	46	3.7	57	28
37	47	7	28	28
37	48	7	20	20
37	49	12	28	28
37	50	11	28	28
37	51	11	21	21
37	52	==		
37	53	5.8	36	28
37	54	==		
37	55	==		
37	56	==		
37	57	==		
37	58	1.8	22	21
37	59	1	22	22
37	60	0.16	23	22
37	61	0.016	23	23

^aA complete set of data for the reaction $1 A \text{ GeV } ^{238}\text{U}$ on protons (this work, [11–13]) are collected in Ref. [49]. There, the values for $Z < 28$ are taken from the present work, the values for the isotopes of the elements $Z = 28$ and $Z = 29$ are obtained from the combination of the two experimental results obtained in this work and in Ref. [12], and for the nuclei above $Z = 30$ and $Z = 37$ the data of Ref. [12] are presented.

TABLE A2. Measured mean velocities for the fission fragments from the spallation of $1 A \text{ GeV } ^{238}\text{U}$ on hydrogen.

Z of fission fragment	Mean recoil velocity of mother nuclei in the beam frame (cm/ns)	Mean velocity in mother-nucleus frame (cm/ns)	Mean kinetic energy in the mother-nucleus frame (MeV)
17	-0.13 ± 0.02	2.00 ± 0.03	77.9 ± 0.8
18	-0.09 ± 0.02	1.99 ± 0.03	82.4 ± 1.2
19	-0.13 ± 0.01	1.94 ± 0.02	83.4 ± 1.3
20	-0.12 ± 0.01	1.88 ± 0.01	82.0 ± 1.4
21	-0.12 ± 0.01	1.86 ± 0.02	84.8 ± 1.6
22	-0.13 ± 0.01	1.83 ± 0.02	86.1 ± 0.6
23	-0.13 ± 0.01	1.80 ± 0.01	87.2 ± 1.3
24	-0.12 ± 0.01	1.76 ± 0.01	86.8 ± 1.2
25	-0.10 ± 0.01	1.71 ± 0.03	85.9 ± 1.2
26	-0.12 ± 0.01	1.70 ± 0.01	87.9 ± 1.0
27	-0.10 ± 0.01	1.67 ± 0.01	88.8 ± 1.3
28	-0.12 ± 0.01	1.61 ± 0.01	86.9 ± 0.9
29	-0.11 ± 0.01	1.60 ± 0.01	89.3 ± 1.4
30	-0.11 ± 0.01	1.57 ± 0.01	88.8 ± 0.5
31	-0.10 ± 0.01	1.55 ± 0.01	90.6 ± 1.4
32	-0.12 ± 0.01	1.49 ± 0.02	86.2 ± 1.2
33	-0.12 ± 0.01	1.46 ± 0.02	86.3 ± 1.5
34	-0.12 ± 0.01	1.44 ± 0.02	86.3 ± 1.4
35	-0.11 ± 0.01	1.42 ± 0.01	86.9 ± 1.2
36	-0.12 ± 0.01	1.38 ± 0.02	84.9 ± 1.2
37	-0.12 ± 0.01	1.36 ± 0.01	84.4 ± 1.4
38	-0.11 ± 0.01	1.35 ± 0.02	77.9 ± 0.8
39	-0.12 ± 0.01	1.29 ± 0.01	82.4 ± 1.2

- [1] C. Rubbia, J. A. Rubio, S. Buono, F. Carminati, N. Fiétier, J. Gálvez, C. Gelès, Y. Kadi, R. Klapisch, P. Mandrillon, J. P. C. Revol, and C. Roche, Internal Report CERN, CERN/AT-95-44 (ET) September 1995.
- [2] D. Ridikas, W. Mittig, and N. Alamanos, Internal Report CEA France, DAPNIA-SPHN-2000-59 August 2000.
- [3] R. Michel and P. Nagel, International Codes and Model Intercomparison for Intermediate Energy Activation Yields, NSC/DOC(97)-1, NEA/P&T No. 14, 1997.
- [4] F. Rejmund, B. Mustapha, P. Armbruster, J. Benlliure, M. Bernas, A. Boudard, J. P. Dufour, T. Enqvist, R. Legrain, S. Leray, K.-H. Schmidt, C. Stéphan, J. Taieb, L. Tassan-Got, and C. Volant, Nucl. Phys. **A683**, 540 (2001).
- [5] J. Benlliure, P. Armbruster, M. Bernas, A. Boudard, J. P. Dufour, T. Enqvist, R. Legrain, S. Leray, B. Mustapha, F. Rejmund, K.-H. Schmidt, C. Stéphan, L. Tassan-Got, and C. Volant, Nucl. Phys. **A683**, 513 (2001).
- [6] T. Enqvist, W. Wlazlo, P. Armbruster, J. Benlliure, M. Bernas, A. Boudard, S. Czajkowski, R. Legrain, S. Leray, B. Mustapha, M. Pravikoff, F. Rejmund, K.-H. Schmidt, C. Stéphan, J. Taieb, L. Tassan-Got, and C. Volant, Nucl. Phys. **A686**, 481 (2001).
- [7] T. Enqvist, P. Armbruster, J. Benlliure, M. Bernas, A. Boudard, S. Czajkowski, R. Legrain, S. Leray, B. Mustapha, M. Pravikoff, F. Rejmund, K.-H. Schmidt, C. Stéphan, J. Taieb, L. Tassan-Got, F. Vivès, C. Volant, and W. Wlazlo, Nucl. Phys. **A703**, 435 (2002).
- [8] A. Kelic, K.-H. Schmidt, T. Enqvist, A. Boudard, P. Armbruster, J. Benlliure, M. Bernas, S. Czajkowski, R. Legrain, S. Leray, B. Mustapha, M. Pravikoff, F. Rejmund, C. Stephan, J. Taieb, L. Tassan-Got, C. Volant, and W. Wlazlo, Phys. Rev. C **70**, 064608 (2004).
- [9] B. Fernandez-Dominguez, P. Armbruster, L. Audouin, J. Benlliure, M. Bernas, A. Boudard, E. Casarejos, S. Czajkowski, J. E. Ducret, T. Enqvist, B. Jurado, R. Legrain, S. Leray, B. Mustapha, J. Pereira, M. Pravikoff, F. Rejmund, M. V. Ricciardi, K.-H. Schmidt, C. Stephan, J. Taeb, L. Tassan-Got, C. Volant, and W. Wlazlo, Nucl. Phys. **A747**, 227 (2005).
- [10] L. Audouin, L. Tassan-Got, P. Armbruster, J. Benlliure, M. Bernas, A. Boudard, E. Casarejos, S. Czajkowski, T. Enqvist, B. Fernandez-Dominguez, B. Jurado, R. Legrain, S. Leray, B. Mustapha, J. Pereira, M. Pravikoff, F. Rejmund, M. V. Ricciardi, K.-H. Schmidt, C. Stephan, J. Taieb, C. Volant, and W. Wlazlo, arXiv nucl-ex/0503021.
- [11] J. Taeb, K.-H. Schmidt, L. Tassan-Got, P. Armbruster, J. Benlliure, M. Bernas, A. Boudard, E. Casarejos, S. Czajkowski, T. Enqvist, R. Legrain, S. Leray, B. Mustapha, M. Pravikoff, F. Rejmund, C. Stéphan, C. Volant, and W. Wlazlo, Nucl. Phys. **A724**, 413 (2003).
- [12] M. Bernas, P. Armbruster, J. Benlliure, A. Boudard, E. Casarejos, S. Czajkowski, T. Enqvist, R. Legrain, S. Leray, B. Mustapha, P. Napolitani, J. Pereira, F. Rejmund, M.-V. Ricciardi, K.-H. Schmidt, C. Stéphan, J. Taieb, L. Tassan-Got, and C. Volant, Nucl. Phys. **A725**, 213 (2003).
- [13] M. Bernas, P. Armbruster, J. Benlliure, A. Boudard, E. Casarejos, T. Enqvist, A. Kelic, R. Legrain, S. Leray, J. Pereira, F. Rejmund, M.-V. Ricciardi, K.-H. Schmidt, C. Stéphan, J. Taieb, L. Tassan-Got, and C. Volant, Nucl. Phys. **A765**, 197 (2006).
- [14] E. Casarejos, Ph.D. thesis, Universidad de Santiago de Compostela, Spain, 2001, GSI Diss-04-2002.
- [15] J. Pereira, Ph.D. thesis, Universidad de Santiago de Compostela, Spain, 2004.
- [16] C. Villagrasa, Ph.D. thesis, University of Paris XI, France, 2003.
- [17] P. Napolitani, Ph.D. thesis, University of Paris XI, France, 2004.
- [18] K.-H. Schmidt, E. Hanelt, H. Geissel, G. Münzenberg, and J. P. Dufour, Nucl. Instrum. Methods A **260**, 287 (1987).
- [19] An International Accelerator Facility for Beams of Ions and Antiprotons, Conceptual Design Report, Publ. GSI, November 2001, <http://www.gsi.de/fair/reports/index.e.html>.
- [20] P. Armbruster, J. Benlliure, M. Bernas, A. Boudard, E. Casarejos, S. Czajkowski, T. Enqvist, S. Leray, P. Napolitani, J. Pereira, F. Rejmund, M. V. Ricciardi, K.-H. Schmidt, C. Stéphan, J. Taeb, L. Tassan-Got, and C. Volant, Phys. Rev. Lett. **93**, 212701 (2004).
- [21] Ch. Engelmann, Ph.D. thesis, University Tübingen, Germany, 1998.
- [22] M. Bernas, C. Engelmann, P. Armbruster, S. Czajkowski, F. Ameil, C. Böckstiegel, Ph. Dessagne, C. Donzaud, H. Geissel, A. Heinz, Z. Janas, C. Kozhuharov, Ch. Mische, G. Münzenberg, M. Pfützner, W. Schwab, C. Stephan, K. Sümmerer, L. Tassan-Got, and B. Voss, Phys. Lett. **B415**, 111 (1997).
- [23] Ch. Engelmann, F. Ameil, P. Armbruster, M. Bernas, S. Czajkowski, Ph. Dessagne, C. Donzaud, H. Geissel, A. Heinz, Z. Janas, C. Kozhuharov, Ch. Mische, G. Münzenberg, M. Pfützner, C. Röhl, W. Schwab, C. Stephan, K. Sümmerer, L. Tassan-Got, and B. Voss, Z. Phys. A **352**, 351 (1995).
- [24] J. S. George, R. A. Mewaldt, N. E. Yanasak, M. E. Wiedenbeck, J. J. Connell, L. Audouin, C.-O. Bacri, B. Berthier, L. Ferrant, F. Rejmund, C. Stephan, L. Tassan-Got, D. Karamanis, S. Czajkowski, A. Boudard, J.-E. Ducret, B. Fernandez, S. Leray, C. Villagrasa, C. Volant, T. Faestermann, T. Enqvist, F. Hammache, K. Helariutta, B. Jurado, K.-H. Schmidt, K. Sümmerer, M. V. Ricciardi, F. Vives, A. Heinz, J. Benlliure, E. Casarejos, M. F. Ordonez, J. Pereira-Conca, and A. R. Junghans, in *Proceedings of the 27th International Cosmic Ray Conference, Hamburg, Germany*, edited by K.-H. Kampert, G. Heinzemann, and C. Spiering (Publ. Copernicus Gesellschaft), Vol. 5 (2001), p. 1956.
- [25] J. M. Alexander, C. Baltzinger, and M. F. Gazdik, Phys. Rev. **129**, 1826 (1963).
- [26] V. P. Crespo, J. B. Cumming, and A. M. Poskanzer, Phys. Rev. **174**, 1455 (1968).
- [27] K. Beg and T. Porile, Phys. Rev. C **3**, 1631 (1971).
- [28] B. N. Belyaev, V. D. Domkin, Yu. G. Korobulin, L. N. Androneko, and G. E. Solyakin, Nucl. Phys. **A348**, 479 (1980).
- [29] A. S. Botvina, I. N. Mishustin, M. Begemann-Blaich, J. Hubele, G. Imme, I. Iori, P. Kreutz, G. J. Kunde, W. D. Kunze, V. Lindenstruth, U. Lynen, A. Moroni, W. F. J. Müller, C. A. Ogilvie, J. Pochodzalla, G. Raciti, Th. Rubehn, H. Sann, A. Schüttauf, W. Seidel, W. Trautmann, and A. Wörner, Nucl. Phys. **A584**, 737 (1995).
- [30] A. A. Kotov, L. N. Andronenko, M. N. Andronenko, Y. I. Gusev, K. V. Lukashin, W. Neubert, D. M. Seliverstov, I. I. Strakovsky, and L. A. Vaishnene, Nucl. Phys. **A583**, 575 (1995).

- [31] H. W. Barz, J. P. Bondorf, H. Schulz, L. N. Andronenko, A. A. Kotov, L. A. Vaishnena, and W. Neubert, *Nucl. Phys.* **A460**, 714 (1986).
- [32] P. Chesny, A. Forgeas, J. M. Gheller, G. Guiller, P. Pariset, L. Tassan-Got, P. Armbruster, K.-H. Behr, J. Benlliure, K. Burkard, A. Brünle, T. Enqvist, F. Farget, and K.-H. Schmidt, *GSI 97-1* 190 (1997).
- [33] H. Geissel, P. Armbruster, K. H. Behr, A. Brünle, K. Burkard, M. Chen, H. Folger, B. Franczak, H. Keller, O. Klepper, B. Langenbeck, F. Nickel, E. Pfeng, M. Pfützner, E. Roeckl, K. Rykaczewski, I. Schall, D. Schardt, C. Scheidenberger, K.-H. Schmidt, A. Schröter, T. Schwab, K. Sümmerer, M. Weber, and G. Münzenberg, *Nucl. Instrum. Methods B* **70**, 286 (1992).
- [34] B. Voss, T. Brohm, H. G. Clerc, A. Grewe, E. Hanelt, A. Heinz, M. de Jong, A. Junghans, W. Morawek, C. Röhl, S. Steinhäuser, C. Ziegler, K.-H. Schmidt, K.-H. Behr, H. Geissel, G. Münzenberg, F. Nickel, C. Scheidenberger, K. Sümmerer, A. Magel, and M. Pfützner, *Nucl. Instrum. Methods A* **364**, 150 (1995).
- [35] M. Pfützner, H. Geissel, G. Münzenberg, F. Nickel, Ch. Scheidenberger, K. H. Schmidt, K. Sümmerer, T. Brohm, B. Voss, and H. Bichsel, *Nucl. Instrum. Methods B* **86**, 213 (1994).
- [36] M. de Jong, K.-H. Schmidt, B. Blank, C. Böckstiegel, T. Brohm, H.-G. Clerc, S. Czajkowski, M. Dornik, H. Geissel, A. Grewe, E. Hanelt, A. Heinz, H. Irnich, A. R. Junghans, A. Magel, G. Münzenberg, F. Nickel, M. Pfützner, A. Piechaczek, C. Scheidenberger, W. Schwab, S. Steinhäuser, K. Sümmerer, W. Trinder, B. Voss, and C. Ziegler, *Nucl. Phys.* **A628**, 479 (1998).
- [37] T. Enqvist, J. Benlliure, E. Farget, K.-H. Schmidt, P. Armbruster, M. Bernas, L. Tassan-Got, A. Boudard, R. Legrain, C. Volant, C. Böckstiegel, M. de Jong, and J. P. Dufour, *Nucl. Phys.* **A658**, 47 (1999).
- [38] M. V. Ricciardi, Ph.D. thesis, Universidad de Santiago de Compostela, Spain, 2005 (GSI Diss. 2005-7).
- [39] P. Armbruster, M. Bernas, S. Czajkowski, H. Geissel, T. Aumann, P. Dessagne, C. Donzaud, E. Hanelt, A. Heinz, M. Hesse, C. Kozhuharov, Ch. Miehé, G. Münzenberg, M. Pfützner, K. H. Schmidt, W. Schwab, C. Stéphan, K. Sümmerer, L. Tassan-Got, and B. Voss, *Z. Phys. A* **355**, 191 (1996).
- [40] C. Donzaud, S. Czajkowski, P. Armbruster, M. Bernas, C. Böckstiegel, Ph. Dessagne, H. Geissel, E. Hanelt, A. Heinz, C. Kozhuharov, Ch. Miehé, G. Münzenberg, M. Pfützner, W. Schwab, C. Stéphan, K. Sümmerer, L. Tassan-Got, and B. Voss, *Eur. Phys. J. A* **1**, 407 (1998).
- [41] W. Schwab, M. Bernas, P. Armbruster, S. Czajkowski, Ph. Dessagne, C. Donzaud, H. Geissel, A. Heinz, C. Kozhuharov, Ch. Miehé, G. Münzenberg, M. Pfützner, C. Stéphan, K. Sümmerer, L. Tassan-Got, and B. Voss, *Eur. Phys. J. A* **2**, 179 (1998).
- [42] J. Hüfner, *Phys. Rep.* **125**, 129 (1985).
- [43] A. S. Goldhaber, *Phys. Lett.* **B53**, 306 (1974).
- [44] D. J. Morrissey, *Phys. Rev. C* **39**, 460 (1989).
- [45] M. V. Ricciardi, T. Enqvist, J. Pereira, J. Benlliure, M. Bernas, E. Casarejos, V. Henzl, A. Kelic, J. Taieb, and K.-H. Schmidt, *Phys. Rev. Lett.* **90**, 212302 (2003).
- [46] J. Benlliure, J. Pereira-Conca, and K.-H. Schmidt, *Nucl. Instrum. Methods A* **478**, 493 (2002).
- [47] M. V. Ricciardi, A. V. Ignatyuk, A. Kelic, P. Napolitani, F. Rejmund, K.-H. Schmidt, and O. Yordanov, *Nucl. Phys.* **A733**, 299 (2004).
- [48] M. Bernas, E. Casarejos, J. Pereira, M. V. Ricciardi, J. Taieb, P. Armbruster, J. Benlliure, A. Boudard, S. Czajkowski, T. Enqvist, R. Legrain, S. Leray, B. Mustapha, M. Pravikoff, F. Rejmund, K.-H. Schmidt, C. Stéphan, L. Tassan-Got, C. Volant, and W. Wlazlo, Report on the progress of the HINDAS Work Package 6, GSI Report 2002-05, September 2002.
- [49] <http://www-w2k.gsi.de/charms/data.htm>
- [50] J. P. Dufour, R. Del Moral, H. Emmermann, F. Hubert, D. Jean, C. Poinot, M. S. Pravikoff, A. Fleury, H. Delagrangé, and K.-H. Schmidt, *Nucl. Instrum. Methods A* **248**, 267 (1986).
- [51] <http://www-wnt.gsi.de/charms/amadeus.htm>
- [52] K.-H. Schmidt, S. Steinhäuser, C. Böckstiegel, A. Grewe, A. Heinz, A. R. Junghans, J. Benlliure, H.-G. Clerc, M. de Jong, J. Müller, M. Pfützner, and B. Voss, *Nucl. Phys.* **A665**, 221 (2000).
- [53] F. Gönnenwein, in *The Nuclear Fission Process*, edited by C. Wagemans (CRC Press, Inc. Boca Raton, 1991), p. 409.
- [54] M. Bernas, P. Armbruster, S. Czajkowski, H. Faust, J. P. Bocquet, and R. Brissot, *Phys. Rev. Lett.* **67**, 3661 (1993).
- [55] B. N. Belyaev, V. D. Domkin, Yu. G. Korobulin, L. N. Androneko, and G. E. Solyakin, *Nucl. Phys.* **A348**, 479 (1980).
- [56] R. Klapisch, *Annu. Rev. Nucl. Sci.* **19**, 33 (1969).
- [57] *ISOLDE Users' Guide*, edited by H.-J. Kluge (Publ. CERN, Geneva, 1986, CERN-86-05).
- [58] A. V. Prokofiev, *Nucl. Instrum. Methods A* **463**, 557 (2001).
- [59] A. A. Caretto, J. Hudis, and G. Friedlander, *Phys. Rev.* **110**, 1130 (1958).
- [60] R. Wolfgang, E. W. Baker, A. A. Caretto, J. B. Cumming, G. Friedlander, and J. Hudis, *Phys. Rev.* **103**, 394 (1956).
- [61] J. R. Grover, *Phys. Rev.* **126**, 1540 (1962).
- [62] S. Katcoff, H. R. Fickel, and A. Wyttenbach, *Phys. Rev.* **166**, 1147 (1968).
- [63] G. English, N. T. Porile, and E. P. Steinberg, *Phys. Rev. C* **10**, 2268 (1974).
- [64] S. B. Kaufman and E. P. Steinberg, *Phys. Rev. C* **22**, 167 (1980).
- [65] L. N. Andronenko, L. A. Vaishnena, A. A. Kotov, M. M. Nesterov, N. A. Tarasov, and V. Neubert, *Fiz. Elem. Chastits At. Yadra* **18**, 685 (1987) [*Sov. J. Part. Nucl.* **18**, 289 (1987)].
- [66] W. E. Nervi and G. T. Seaborg, *Phys. Rev.* **97**, 1092 (1955).
- [67] P. Hofmann, A. S. Iljinov, Y. S. Kim, M. V. Mebel, H. Daniel, P. David, T. von Egidy, T. Haninger, F. J. Hartmann, J. Jastrzebski, W. Kurcewicz, J. Lieb, H. Machner, H. S. Plendl, G. Riepe, B. Wright, and K. Ziocck, *Phys. Rev. C* **49**, 2555 (1994).
- [68] D. G. Sarantites, D. R. Bowman, G. J. Wozniak, R. J. Charity, Z. H. Liu, R. J. McDonald, M. A. McMahan, and L. G. Moretto, *Phys. Lett.* **B218**, 427 (1989).
- [69] A. M. Zolotov, B. A. Bochagov, L. N. Andronenko, and G. E. Solyakin, *Yad. Fiz.* **18**, 29 (1973) [*Sov. J. Nucl. Phys.* **18** (1974) 15].
- [70] G. D. Westfall, R. G. Sextro, A. M. Poskanzer, A. M. Zebelman, G. W. Butler, and E. K. Hyde, *Phys. Rev. C* **17**, 1368 (1978).
- [71] N. Bohr and J. A. Wheeler, *Phys. Rev.* **56**, 426 (1939).
- [72] U. L. Businaro and S. Gallone, *Nuovo Cimento* **5**, 315 (1957).

- [73] L. G. Moretto and G. Wozniak, LBL-25744, 1988.
- [74] M. G. Itkis and A. Ya. Rusanov, *Phys. Part. Nucl.* **29**, 160 (1998).
- [75] A. V. Ignatyuk, *Yad. Fiz.* **9**, 357 (1969) [*Sov. J. Nucl. Phys.* **9**, 208 (1969)].
- [76] L. G. Moretto, *Nucl. Phys.* **A247**, 211 (1975).
- [77] W. J. Swiatecki, *Aust. J. Phys.* **36**, 641 (1983).
- [78] R. G. Stokstad, in *Treatise on Heavy-Ion Science*, Vol. 3, edited by D. A. Bromley (Plenum Press, New York, 1988), pp. 83–197.
- [79] A. J. Cole, *Statistical Models for Nuclear Decay: From Evaporation to Vaporisation* (Iop Publ., Bristol, 2000).
- [80] B. D. Wilkins, E. P. Steinberg, and R. R. Chasman, *Phys. Rev. C* **14**, 1832 (1976).
- [81] C. Böckstiegel, S. Steinhäuser, J. Benlliure, H.-G. Clerc, A. Grewe, A. Heinz, M. de Jong, A. R. Junghans, J. Müller, and K.-H. Schmidt, *Phys. Lett.* **B398**, 259 (1997).
- [82] R. Bass, in *Proceedings of the Symposium on Deep-Inelastic and Fusion Reactions with Heavy Ions, Berlin 1979* (Springer-Verlag, Berlin, 1979).
- [83] R. Bass, *Nuclear Reactions with Heavy Ions* (Springer-Verlag, Berlin, 1980).
- [84] V. E. Viola, K. Kwiatkowski, and M. Walker, *Phys. Rev. C* **31**, 1550 (1985).
- [85] O. A. P. Tavares and M. L. Terranova, *II Nuovo Cimento A* **105**, 723 (1992).
- [86] J. Benlliure, A. R. Junghans, B. Jurado, M. V. Ricciardi, and K.-H. Schmidt, *GSI Annual Report 1999, GSI 2000–1*, p. 29.
- [87] J.-J. Gaimard and K.-H. Schmidt, *Nucl. Phys.* **A531**, 709 (1991).
- [88] A. R. Junghans, M. de Jong, H.-G. Clerc, A. V. Ignatyuk, G. A. Kudyaev, and K.-H. Schmidt, *Nucl. Phys.* **A629**, 635 (1998).
- [89] J. Benlliure, A. Grewe, M. de Jong, K.-H. Schmidt, and S. Zhdanov, *Nucl. Phys.* **A628**, 458 (1998).
- [90] J. Cugnon, C. Volant, and S. Vuillier, *Nucl. Phys.* **A620**, 475 (1997).
- [91] B. Jurado, C. Schmitt, K.-H. Schmidt, J. Benlliure, and A. R. Junghans, *Nucl. Phys.* **A747**, 14 (2005).
- [92] S. I. Mulgin, K.-H. Schmidt, A. Grewe, and S. V. Zhdanov, *Nucl. Phys.* **A640**, 375 (1998).
- [93] A. V. Ignatyuk, K. K. Istekov, and G. N. Smirenkin, *Yad. Fiz.* **29**, 875 (1979) [*Sov. J. Nucl. Phys.* **29**, 450 (1979)].
- [94] R. J. Charity, M. A. McMahan, G. J. Wozniak, R. J. McDonald, L. G. Moretto, D. G. Sarantites, L. G. Sobotka, G. Guarino, A. Pantaleo, L. Fiore, A. Gobbi, and K. D. Hildenbrand, *Nucl. Phys.* **A483**, 371 (1988).
- [95] M. Kildir, G. La Rana, R. Moro, A. Brondi, E. Vardaci, A. D’Onofrio, D. Fessas, E. Perillo, V. Roca, M. Romano, F. Terrasi, G. Nebbia, G. Viesti, and G. Prete, *Phys. Rev. C* **51**, 1873 (1995).
- [96] P. Armbruster, *Nucl. Phys.* **A140**, 385 (1970).
- [97] F. Atchinson, “Spallation and Fission in Heavy Metal Nuclei under Medium Energy Proton Bombardment,” in *Proc. Meeting on Targets for Neutron Beam Spallation Sources*, Jülich, June 11–12, 1979, pp. 17–46, edited by G. S. Bauer, Publ. KFA Jülich GmbH, Jülich Germany, 1980.
- [98] D. Ridikas, in *Proceedings of the 3rd International Workshop on Nuclear Fission and Fission-Product Spectroscopy*, 11–15 May, 2005, Cadarache, France (unpublished).
- [99] T. A. Bredeweg, R. Yanez, B. P. Davin, K. Kwiatkowski, R. T. de Souza, R. Lemmon, R. Popescu, R. J. Charity, L. G. Sobotka, D. Hofman, and N. Carjan, *Phys. Rev. C* **66**, 014608 (2002).
- [100] P. Wagner, J. Richert, V. A. Karnaukhov, and H. Oeschler, *Phys. Lett.* **B460**, 31 (1999).
- [101] A. Schüttauf, W. D. Kunze, A. Wörner, M. Begemann-Blaich, Th. Blaich, D. R. Bowman, R. J. Charity, A. Cosmo, A. Ferrero, C. K. Gelbke, C. Groß, W. C. Hsi, J. Hubele, G. Imme, I. Iori, J. Kempter, R. Kreuz, G. J. Kunde, V. Lindenstruth, M. A. Lisa, W. G. Lynch, U. Lynen, M. Mang, T. Möhlenkamp, A. Moroni, W. F. J. Müller, M. Neumann, B. Ocker, C. A. Ogilvie, G. F. Peaslee, J. Pochodzalla, G. Raciti, F. Rosenberger, Th. Rubehn, H. Sann, C. Schwarz, W. Seidel, V. Serfling, L. G. Sobotka, J. Stroth, L. Stuttge, S. Tomasevic, W. Trautmann, A. Trzcinski, M. B. Tsang, A. Tucholski, G. Verde, C. W. Williams, E. Zude, and B. Zwieglinski, *Nucl. Phys.* **A607**, 457 (1996).
- [102] T. Odeh, R. Bassini, M. Begemann-Blaich, S. Fritz, S. J. Gaff-Ejakov, D. Gourio, C. Groß, G. Immé, I. Iori, U. Kleinevoß, G. J. Kunde, W. D. Kunze, U. Lynen, V. Maddalena, M. Mahi, T. Möhlenkamp, A. Moroni, W. F. J. Müller, C. Nociforo, B. Ocker, F. Petruzzelli, J. Pochodzalla, G. Raciti, G. Riccobene, F. P. Romano, A. Saija, M. Schnittker, A. Schüttauf, C. Schwarz, W. Seidel, V. Serfling, C. Sfienti, W. Trautmann, A. Trzcinski, G. Verde, A. Wörner, Hongfei Xi, and B. Zwieglinski, *Phys. Rev. Lett.* **84**, 4557 (2000).
- [103] W. Lang, H.-G. Clerc, H. Wohlfarth, H. Schrader, and K.-H. Schmidt, *Nucl. Phys.* **A345**, 34 (1980).
- [104] U. Jahnke, W. Bohne, T. von Egidy, P. Figuera, J. Galin, F. Goldenbaum, D. Hilscher, J. Jastrzebski, B. Lott, M. Morjean, G. Pausch, A. Peghaire, L. Pienkowski, D. Polster, S. Proschitzki, B. Quednau, H. Rossner, S. Schmid, and W. Schmid, *Phys. Rev. Lett.* **83**, 4959 (1999).
- [105] B. Lott, F. Goldenbaum, A. Boehm, W. Bohne, T. von Egidy, P. Figuera, J. Galin, D. Hilscher, U. Jahnke, J. Jastrzebski, M. Morjean, G. Pausch, A. Péghaire, L. Pienkowski, D. Polster, S. Proschitzki, B. Quednau, H. Rossner, S. Schmid, and W. Schmid, *Phys. Rev. C* **63**, 034616 (2001).